ADVANCED COMPOSITES LETTERS

Original Research Article

Advanced Composites Letters
Volume 29: 1–22

DOI: 10.1177/0963693520941865
journals.sagepub.com/home/acm
SAGE

Three new hybrid quasi-3D and 2D higher-order shear deformation theories for free vibration analysis of functionally graded material monolayer and sandwich plates with stretching effect

Y Belkhodja[1,2], D Ouinas[1], H Fekirini[2], JA Viña Olay[3] and M Touahmia[4]

Abstract

The present investigation brings to the readers three new hybrid higher-order shear deformation theory (HSDT) models and analyses the functionally graded material (FGM) plates. The major objective of this work is to develop three HSDTs in a unique formulation by polynomial–hyperbolic–exponential and polynomial–trigonometric forms, propose the three new HSDT models, investigate the effect of thickness stretching by considering a quasi-three-dimensional theory and analyse the free vibration of isotropic and FGM monolayer and sandwich (symmetric as well as non-symmetric, with hardcore as well as softcore) plates to demonstrate the models ability. Therefore, the Hamilton's principle is exploited to develop equations of motion based on a displacement field of only five unknowns, of which three of them distinguished the transverse displacement membranes through the plate thickness (bending, shear and stretching displacements). In addition, the analytical solutions are found by applying the Navier approach for a simply supported boundary conditions type. The theory also considered that transverse shear deformation effect satisfied the stress-free boundary conditions on the plate-free surfaces without any requirement of shear correction factors. The used mechanical properties followed the power law and the Mori–Tanaka scheme distributions through the plate thickness. The determined results explained the effects of different non-dimensional parameters, and the proposed HSDTs predict the proper responses for monolayer and sandwich (symmetric as well as non-symmetric, with hardcore as well as softcore) FGM plates in comparison with other different plates' theories solutions found in the literature references, thus the reliability and accuracy of the present approach are ascertained. It is obtained that the present formulations of polynomial–hyperbolic–exponential and polynomial–trigonometric forms can be further extended to all existing HSDTs models, for numerous problems related to the shear deformable effect.

Keywords

quasi-3D and 2D HSDTs, FGM monolayer and sandwich plates, free vibration, stretching effect, analytical model

[1] LMNEPM, Numerical and Experimental Modelling of the Mechanical Phenomena Laboratory, Mechanical Engineering Department, Faculty of Sciences and Technology, Abdelhamid Ibn Badis University, Mostaganem, Algeria
[2] LMPM, Mechanics and Physics of Materials Laboratory, Mechanical Engineering Department, Faculty of Technology, Djillali Liabes University, Sidi Bel Abbes, Algeria
[3] Materials Science and Metallurgical Engineering Department, University of Oviedo, Viesques Campus, Gijón, Asturias, Spain
[4] Civil Engineering Department, College of Engineering, University of Hail, Saudi Arabia

Date received: 4 March 2020; accepted: 22 June 2020

Corresponding author:
Y Belkhodja, LMNEPM, Numerical and Experimental Modelling of the Mechanical Phenomena Laboratory, Mechanical Engineering Department, Faculty of Sciences and Technology, Abdelhamid Ibn Badis University, Mostaganem 27000, Algeria; LMPM, Mechanics and physics of materials Laboratory, Mechanical Engineering Department, Faculty of Technology, Djillali Liabes University, Sidi Bel Abbes 22000, Algeria.
Emails: yamna.belkhodja@univ-sba.dz; belkhodjayamna44@gmail.com

Introduction

Functionally graded materials (FGMs) are a new generation of the composite materials (ceramic/metal) that were developed by a Japanese material scientists group from National Aerospace Laboratories in 1984, as a means of preparing thermal barrier materials.[1] These materials have been given great popularity in the design, fabrication and development research fields, after the first national project entitled 'Research on the Basic Technology for the Development of FGMs for Relaxation of Thermal-Stress', because of their considerable thermal and mechanical capabilities.[2–12] Their richer compositions of ceramic qualified them to be used in sectors of extremely high temperature, such as aeronautical structures, space aircraft and nuclear enclosures. The used FGM plates and shells avoid several problems in classical composite materials, especially during dynamic or cyclic loadings, such as the delamination problem. However, they are subjected to the vibration problem. As a result, these problems have been treated by many analytical and numerical studies based on different plate theories that were developing in three phases, which are the classical plate theory (CPT), the first-order shear deformation theory (FSDT) that requires a shear correction factor, as well the higher-order shear deformation theory (HSDT) that includes a shear deformation effect, such as the sinusoidal higher-order shear deformation theory (SSDT), which was used by a two-dimensional (2D) HSDT derived by Matsunaga.[13] He analysed the free vibration problem by a method of power series expansion of displacements components, and a set of fundamental dynamic equations, for rectangular FGM plates with simply supported edges. Belabed et al.[14] presented a hyperbolic HSDT with the stretching effect to predict free vibration responses of FGM plates. They indicated that the thickness stretching effect for thick plates is important. It is noticed that Talha and Singh[15] presented an HSDT for an investigation of the free vibration problem and made a special modification in the transverse displacement in conjunction with finite element models. The obtained results employed a continuous isoparametric Lagrangian finite element with 13 degrees of freedom per node. They used the FGM plates with different boundary conditions. A new HSDT developed by Ait Atmane et al.[16] studied free vibration resting on Winkler–Pasternak elastic foundations analysis of FGM plates. Whereas the higher-order shear and normal deformable plate theory studied by Qian et al.[17] used the meshless local Petrov–Galerkin method. The theory investigated both of the free and forced vibrations analyses of a thick rectangular elastic FGM plate. They used only the Mori–Tanaka homogenization technique to calculate the effective material modules. Younsi et al.[18] developed a new 2D and quasi three-dimensional (quasi-3D) hyperbolic HSDT for the analyses of free vibration problem of FGM plates, and the used displacements field included undetermined integral terms. A new quasi-3D hyperbolic HSDT for the free vibration analysis of functionally graded plates is developed by Hebali et al.[19] Zaoui et al.[20] studied the free vibration of FGM plates resting on elastic foundations based on quasi-3D hybrid-type HSDT. A new SSDT developed by Thai and Thuc[21] analysed the vibration of FGM plates. It can be seen that Neves et al.[22] studied a quasi-3D SSDT for the free vibration problem analysed for FGM plates. A new HSDT developed by Thai and Kim[23] analysed the free vibration problem of FGM plates with simply supported edges. Abedalnour et al.[24] developed a new quasi-3D trigonometric HSDT and a new displacement field that introduced undetermined integral variables for the free vibration analysis of FGM plates with simply supported edges. A quasi-3D SSDT developed by Neves et al.[25] analysed the free vibration problem of the FGM plates. A new quasi-3D hyperbolic HSDT was developed by Neves et al.[26] for the free vibration analysis of FGM plates with simply supported edges. Thai et al.[27] proposed a new inverse tangent shear deformation theory for the free vibration analysis of laminated composite and sandwich plates. In addition, two new shear deformation theories for the free vibration analysis of FGM made of isotropic and sandwich plates are presented by Thai et al..[28] Nguyen-Xuan et al.[29] presented a new fifth-order shear deformation theory for composite sandwich plates and the free vibration analysis of rectangular and circular plates investigated for different boundary conditions. Thai et al.[30] derived a quasi-3D shear deformation theory for free vibration analysis of multilayer functionally graded graphene platelet-reinforced composite microplates. A new shear and normal deformations theory for the free vibration of FGM isotropic and sandwich plates is presented by Thai et al..[31] Based on an HSDT, Thai et al.[32] presented a non-classical model for the free vibration analysis of FGM isotropic and sandwich microplates. Nebab et al.[33] used an HSDT to predict the free vibration of the FGM plate. A novel quasi-3D HSDT constructed from a novel seventh-order shear deformation is proposed by Nguyen et al.[34] to investigate the free vibration responses of rectangular and circular FGM microplates. Bennoun et al.[35] developed a new quasi-3D HSDT for the free vibration analysis of FGM sandwich plates. Zaoui et al.[36] proposed a new hybrid 2D and quasi-3D HSDT (exponential–trigonometric), for the free vibration analysis of FGM plates, resting on elastic foundations. An HSDT was studied by Belkhodja et al.[37] for the free vibration analysis of FGM plates with simply supported edges. A new hyperbolic HSDT is presented for the free vibration analysis of FGM sandwich plates by El Meiche et al.[38]

The present study developed three new hybrid quasi-3D and 2D HSDTs (polynomial–hyperbolic–exponential) and (polynomial–trigonometric) for the free vibration problems analysis of square and rectangular FGM monolayer and sandwich (symmetric as well as non-symmetric, with hardcore as well as softcore) plates with simply supported edges. The selected displacements field included the transverse shear deformation effect that satisfied the stress-free boundary conditions on the plate free surfaces, and only five unknowns, which three of them characterized the bending, shear and thickness stretching transverse displacement membranes through the plate thickness. The mechanical properties are

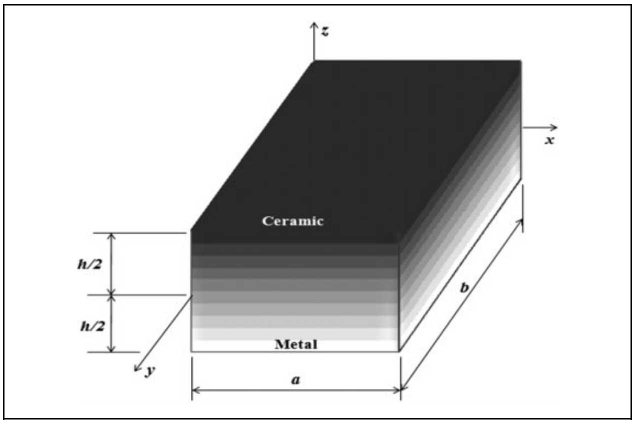

Figure 1. The FGM plate geometric model.[37] FGM: functionally graded material.

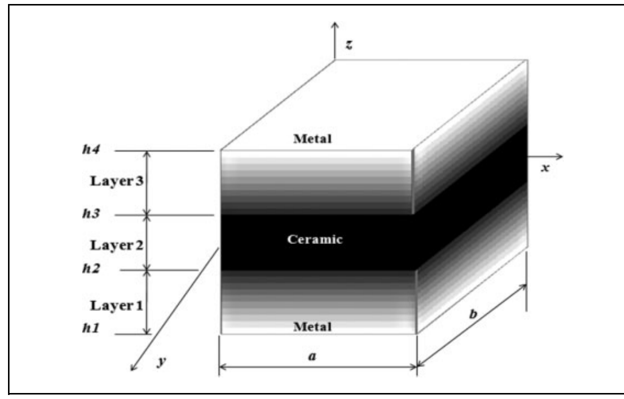

Figure 2. The FGM sandwich plate geometric model (type A). FGM: functionally graded material.

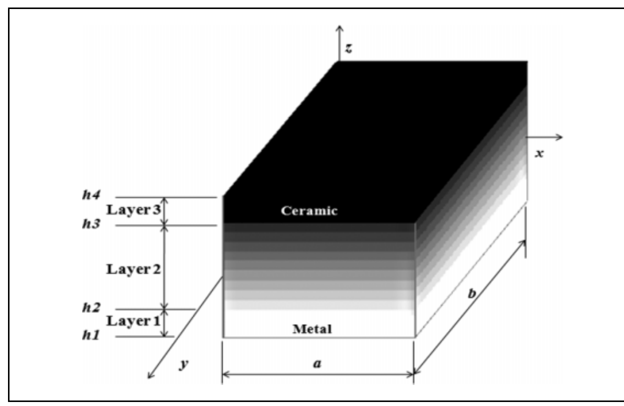

Figure 3. The FGM sandwich plate geometric model (type B). FGM: functionally graded material.

continuously varied through the plate thickness as the power-law (P-FGMs) and the Mori–Tanaka scheme (MT-FGMs) distributions. Moreover, the produced five equations of motion were obtained from Hamilton's principle and were solved by the Navier approach for simply supported boundary conditions. Furthermore, a richer study investigated several parameters effects such as the geometric ratios (the side-to-thickness ratio, the aspect ratio as well the thickness ratio for symmetric and non- symmetric, with hardcore as well as soft-core sandwich plates), the volume fraction index, the frequency modes and the materials properties on the natural frequencies. Finally, analytical solutions were obtained and numerical results were validated by comparisons with others plates' theories solutions found in the literature references to verify the accuracy and the efficiency of the present theories.

The theoretical formulation

An accurate and efficient theoretical formulation is achieved for the FGMs by a developed architecture of design, processing and evaluation.[1] Thus, the used architectural design is a monolayer (single-layer) and sandwich (symmetric as well as non-symmetric, with hardcore as well as softcore) plates of the dimensions indicated as length (a), width (b) and uniform thickness (h) as shown in Figures 1, 2 and 3, respectively. The thickness evolution follows the z-coordinate (z-axis) perpendicular to the rectangular Cartesian coordinates (0, x, y) defined in the plate median plane,[37] and all in-plane edges of the plate are parallel to x and y axes as well as the bottom and top plate faces are at the plate extremities $z = \pm h/2$, with respect to the coordinates $h1$ and $h4$.

The sandwich plates (symmetric as well as non-symmetric, with hardcore as well as softcore) are composed of three elastic isotropic homogeneous and anisotropic microscopically heterogeneous layers (Figures 2 and 3): Layer 1 is a bottom face layer ($z \in [h1, h2]$); layer 2 is a median core layer ($z \in [h2, h3]$); and layer 3 is a top face layer ($z \in [h3, h4]$), where $h2$ and $h3$ are the vertical coordinates of the two median interfaces (Figures 2 and 3).

Therefore, the plates were characterized by geometric ratios such as the side-to-thickness ratio (a/h), the aspect ratio $(a/b)^{37}$ and the thickness ratio. The ratio (a/h) specifies three plate thicknesses that are a thick plate (with a low ratio values such as ($a/h = 2, \sqrt{10}, 5$)), moderately thick plate ($a/h \approx 10$) and a thin plate (with high ratio values such as ($a/h = 20$)). It is necessary to know that the transverse shear deformation effect proportionally varies with the plate thickness value.[37] Moreover, the ratios ($a/b = 1$) and ($a/b \neq 1$) define a square plate and a rectangular plate, respectively.[37] The thickness ratio is denoted by the combination of three numbers i-j-k, the sum of the three numbers is X, each number is assumed to be taken from X as ratio as i/X, j/X, k/X, X represent the number of small thicknesses that the plate is divided to, $h1$ and $h2$ are known. The plate in-plane always must be in the median of the plate, if it is noticed that the in-plane pass in a small thickness of the plate and it divided again, then the other small thicknesses will be divided too, all the new smallest thicknesses must have the same thickness. h1 and h2 will be taken from the new division, initiated by the bottom layer to top as (1-0-1), (2-1-2), (1-1-1), (1-2-1) for symmetric sandwich plates as well as (2-2-1), (2-1-1) for non-

Table 1. The material properties of metal and ceramics.

Materials		Material properties Young's modulus (GPa)	Mass density (kg/m^3)	Poisson's ratio
Metal	Aluminium-1 $(Al)_1$	70	2702	0.3
	Aluminium-2 $(Al)_2$	70	2707	0.3
Ceramics	Zirconia (ZrO_2)	200	5700	0.3
	Alumina (Al_2O_3)	380	3800	0.3

symmetric sandwich plates and so on. There are two types of sandwich plates (symmetric as well as non-symmetric, with hardcore as well as softcore): Type A is composed of homogeneous core layer and FGMs face layers (Figure 2), and vice versa for type B (Figure 3).

For structural and functional uses, FGM concept can be applied to several materials.[1] However, the studied FGM plate was made from a graded mixture of only two different materials, a metal (aluminium: Al) and a ceramic (alumina: Al_2O_3 or zirconia: ZrO_2), of mechanical properties grouped in Table 1.

The mechanical properties of the FGMs

FGM compositions gradually change, resulting in a corresponding modification in the effective mechanical properties,[1] they although heterogeneous are idealized as continue through the plate thickness (z-axis), smoothly with respect to the spatial coordinates.[39] Contrary to a discrete model, the mechanical properties are assumed to be graded by simple continuous material distributions neglecting the microstructure of the plate.[37,40] The mechanical properties are the Young's modulus, the Poisson's ratio and the density, were described from homogeneous plate theories, after homogenized the FGM plate with their effective modules.[37,40]

The Young's modulus. The Young's module ($E(z)$) can be expressed by the rule of mixture and follows the mathematical formulation that describes the power-law,[41] and the Mori–Tanaka scheme,[42,43] according to the equation (1):

$$E^{(n)}(z) = (E_c - E_m)V_c^{(n)}(z) + E_m, \tag{1}$$

where $E^{(n)}$, $V^{(n)}$, (n = 1,2,3) denotes the effective material property and the volume fraction function of layer (n), respectively. For the monolayer plate (n = 1), E_c and E_m are the Young's moduli of the upper (ceramic) and lower (metal) FGM plate faces, respectively. The volume fraction of the ceramic material (V_c) is defined in equations 2 (a–d):

For monolayer plate:

Type P-FGMs:

$$V_{c1}(z) = \left(\frac{1}{2} + \frac{z}{h}\right)^P \tag{2a}$$

Type *MT-FGMs:*

$$V_{c2}(z) = V_{c1}(z)\frac{(3-3\nu)}{(3-3\nu) + (1 - V_{c1}(z))\left(\frac{E_c}{E_m} - 1\right)(1+\nu)} \tag{2b}$$

For sandwich P-FGM plate:

Type A:

$$\begin{cases} V_c^{1}(z) = \left(\dfrac{z - h1}{h2 - h1}\right)^P, \\ V_c^{2}(z) = 1, \\ V_c^{3}(z) = \left(\dfrac{z - h4}{h3 - h4}\right)^P, \end{cases} \tag{2c}$$

Type B:

$$\begin{cases} V_c^{1}(z) = 1, \\ V_c^{2}(z) = \left(\dfrac{1}{2} + \dfrac{z - h2}{h3 - h2}\right)^P, \\ V_c^{3}(z) = 0, \end{cases} \tag{2d}$$

where the positive volume fraction index (p) specifies three plate types, namely the homogeneous ceramic plate ($p = 0$, extremely stiff), the FGM plate (p∈]0,∞[, there is the stiffer P-FGM plates (p∈]0,1[), the moderately stiff P-FGM plates ($p = 1$) as well as the softer P-FGM plates (p∈]1,∞[) and the metal plate (p→∞, extremely soft),[37] as well FGM distributions profiles through the plate thickness z∈[-$h/2$, $h/2$] only, follow the volume fractions (V_c), continuously and gradually varied as a function of the position (z-coordinate), as presented in Figure 4 (a) and (b).[37]

The Poisson's ratio. When the Poisson's ratios (ν (z)) of the ceramic and the metal are nearly equal, the Poisson's ratio is considered constant because there is no significant difference between obtained results, and it has no significant effect on the FGM plate.[43,44]

The density (the mass density). The effective density ($\rho(z)$) is estimated only by the power law with Voigt's mixtures rule[45] as:

$$\rho^{(n)}(z) = (\rho_c - \rho_m)V_c^{(n)}(z) + \rho_m \tag{3}$$

The kinematics, the strains, the stresses and the energies study of the present new HSDTs

The kinematics. The present developed HSDTs is a combination of both the procedure were developed for monolayer plates by Belabed et al.,[14] with the used point displacements field extended as the bending (w_b), the shear (w_s) and the stretching (w_{st}) transverse displacement membranes through z-axis, and with only five unknowns (significantly facilitated engineering analyses) as well as the

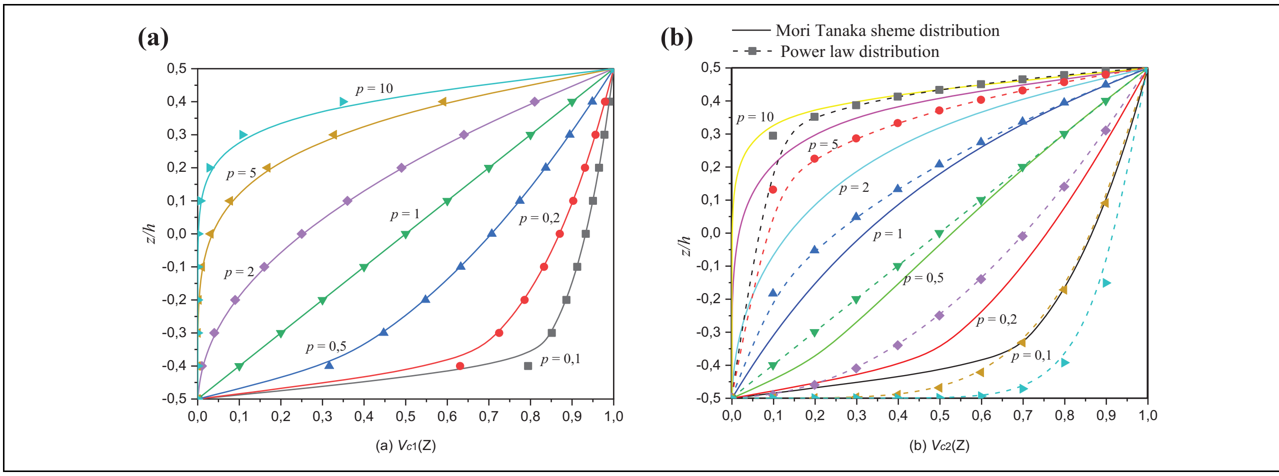

Figure 4. Ceramic material volume fraction: (a) the power law profile $V_{c1}(z) = (z/h + 0.5)^P$ along the thickness of P-FGM plate and (b) the Mori-Tanaka scheme profile along the thickness of MT-FGM plate $V_{c2}(z) = V_{c1}(z).[(3 - 3v)/[(3 - 3v) + (1 - V_{c1}(z))[(E_c - E_m) - 1](1 + v)]]$. P-FGM: power-law functionally graded material; MT-FGM: Mori–Tanaka functionally graded material.

procedures of sandwich (symmetric as well as non-symmetric, with hardcore as well as softcore) plates developed by El Meiche et al.,[38] written as:

$$u(x, y, z, t) = u_0(x, y, t) - z\frac{\partial w_b}{\partial x} - f(z)\frac{\partial w_s}{\partial x} \tag{4a}$$

$$v(x, y, z, t) = v_0(x, y, t) - z\frac{\partial w_b}{\partial y} - f(z)\frac{\partial w_s}{\partial y} \tag{4b}$$

$$w(x, y, z, t) = w_b(x, y, t) + w_s(x, y, t) + w_{st}(x, y, t) \tag{4c}$$

where u_0 and v_0 are, respectively, the axial displacements over the x and y Cartesian coordinates axes on the plate median plane. The developed new hybrid (polynomial–hyperbolic–exponential) and (polynomial–trigonometric) shape functions ($f(z)$) are presented in Table 2, with several other shape functions derived by others researchers illustrating the transverse shear strains and tangential stresses effect nonlinear distribution through the FGM plates thickness (h)[37] and specifies three plates theories displacements field that are the CPT with ($f(z) = 0$), the FSDT[42] with ($f(z) = z$), else the HSDT. Numerical examples are given to show high accuracy of the proposed method in Tables 3 to 8, approved the novelty, simplicity and effectuality of these new HSDTs and shape functions.

The thickness stretching transverse displacement (w_{st}) is defined as

$$w_{st}(x, y, t) = \begin{cases} 0 & \text{For 2D HSDT } (\varepsilon_z = 0). \quad (5a) \\ g(z)\phi(x, y, t) & \text{For 3D and quasi} - \text{3D HSDT } (\varepsilon_z \neq 0). \quad (5b) \end{cases}$$

where an additional term of transverse displacement component φ accounts for the normal deformation effect (stretching effect), and the function $g(z)$ describes thickness stretching effect distribution through the plate thickness and also the transverse shear stress distribution through the same thickness that satisfied and fulfilled the stress-free boundary conditions, as a parabolic variation, as well as it is set to zero at the plate extremities (top and bottom plates surfaces) $z = \pm h/2$.[37]

$$g(z) = 1 - \frac{\mathrm{d}f(z)}{\mathrm{d}z}. \tag{6}$$

The strains. The linear strains field is determined by the linear elasticity theory application based on the displacements field (4) derived as

Table 2. Shape functions form of different higher-order shear deformation theories.

Models		Shape functions *f(z)* of shear strain
Polynomial functions	Ambartsumian[46]	$\frac{zh^2}{8}\left(1-\frac{4}{3}\frac{z^2}{h^2}\right)$
	Kaczkowski[47] Panc[48] Reissner[49]	$\frac{5z}{4}\left(1-\frac{4}{3}\frac{z^2}{h^2}\right)$
	Levinson[50] Murthy[51] Reddy[52]	$z\left(1-\frac{4}{3}\frac{z^2}{h^2}\right)$
	Nguyen-Xuan et al.[29]	$\frac{7}{8}z-\frac{2}{h^2}z^3+\frac{2}{h^4}z^5$
Trigonometric functions	Levy[53] Stein[54] Touratier[55]	$\frac{h}{\pi}\sin\left(\frac{\pi}{h}z\right)$
	Arya et al.[56]	$\sin\left(\frac{\pi}{h}z\right)$
	Thai et al.[27]	$h\arctan\left(\frac{2}{h}z\right)-z$
	Mantari et al.[57]	$\tan(mz)-mz\sec^2\left(\frac{mh}{2}\right), m=\frac{1}{5h}$
	Mantari et al.[57]	$\tan(mz)-mz\sec^2\left(\frac{mh}{2}\right), m=\frac{\pi}{2h}$
	Grover et al.[58]	$z\sec\left(\frac{rz}{h}\right)-z\sec\left(\frac{r}{2}\right)\left(1+\frac{r}{2}\tan\left(\frac{r}{2}\right)\right), r=0.1$
	Grover et al.[58]	$\cot^{-1}\left(\frac{r \quad h}{z}\right)-\frac{4rz}{h(4r^2+1)}, r=0.46$
	Nguyen et al.[59]	$h\tan^{-1}\left(\frac{rz}{h}\right)-\frac{16rz^3}{3h^2(r^2+4)}, r=1$
Hyperbolic functions	Soldatos[60]	$h\sinh\left(\frac{z}{h}\right)-z\cosh\left(\frac{1}{2}\right)$
	El Meiche et al.[38]	$\frac{\frac{h}{\pi}\sinh\left(\frac{\pi}{h}z\right)-z}{\cosh\left(\frac{\pi}{2}\right)-1}$
	Akavci and Tanrikulu[61]	$\frac{3\pi h}{2}\tanh\left(\frac{z}{h}\right)+\frac{3\pi z}{2}\operatorname{sech}^2\left(\frac{1}{2}\right)$
	Akavci and Tanrikulu[61]	$z\operatorname{sech}\left(\frac{\pi z^2}{h^2}\right)-z\operatorname{sech}\left(\frac{\pi}{4}\right)\left(1-\frac{\pi}{2}\tanh\left(\frac{\pi}{4}\right)\right)$
	Mahi et al.[62]	$\frac{h}{2}\tanh\left(\frac{2z}{h}\right)-\frac{4z^3}{3h^2\cosh^2(1)}$
	Grover et al.[63]	$\sinh^{-1}\left(\frac{r \quad z}{h}\right)-\frac{2rz}{h\sqrt{r^2+4}}, r=3$
	Shi et al.[64]	$\frac{h}{2}\tanh\left(\frac{2}{h}z\right)+z\frac{1}{\cosh^2 1}$
Exponential functions	Karama et al.[65]	$ze^{-2\left(\frac{z}{h}\right)^2}$
	Aydogdu[66]	$z\alpha^{-2(z/h)^2/\ln\alpha}=z\left(3^{-2(z/h)^2/\ln 3}\right), \forall\alpha\rangle 0, \alpha$
	Mantari et al.[67]	$m^{-2(z/h)^2}z+y*z=2.85^{-2(z/h)^2}z+0.28z$
Combination functions	Mantari et al.[68]	$\sin\left(\frac{\pi}{h}z\right)e^{\frac{1}{2}\cos\left(\frac{\pi z}{h}\right)}+\frac{\pi}{2h}z$
	Mantari et al.[69]	$\sinh\left(\frac{z}{h}\right)e^{m\cosh\left(\frac{z}{h}\right)}-\frac{z}{h}\left[\cosh\left(\frac{1}{2}\right)+m\sinh^2\left(\frac{1}{2}\right)\right]e^{m\cosh\left(\frac{1}{2}\right)}, m=-6, m=-7$
	Mantari et al.[70]	$ze^{m\cos\left(\frac{nz}{h}\right)}-z\left[1-\frac{1}{2}nm\sin\left(\frac{n}{2}\right)\right]e^{m\cos\left(\frac{n}{2}\right)}, m=1, n=2.9$
	Thai et al.[28]	$\tan^{-1}\left[\sin\left(\frac{\pi z}{h}\right)\right]$
	Thai et al.[28]	$\sinh^{-1}\left[\sin\left(\frac{\pi z}{h}\right)\right]$
	Suganyadevi and Singh[71]	$\frac{h}{r}\tan^{-1}\left(\frac{rz}{h}\right)-\frac{z}{(r^2z^2/h^2)+1}, r=2.5$
	Singh and Singh[72]	$\tan\left(\frac{mz}{h}\right)+2z\cosh\left(\frac{1}{2}\right), m=5$
	Singh and Singh[72]	$\sin\left(\frac{\pi}{h}z\right)+\frac{\pi}{2h}z$
	Zaoui et al.[36] Belkhodja et al.[37]	$\frac{\pi h}{\pi^4+h^4}\left[e^{(hz/\pi)}\left[\pi^2\sin\left(\frac{\pi z}{h}\right)+h^2\cos\left(\frac{\pi z}{h}\right)\right]-h^2\right]$
	Present theory 1	$z\cdot\left(\left(\frac{25z^2}{\pi(z^2h+h^3)}+\cosh\left(\frac{\pi z}{h}\right)+e^{\left(\frac{z}{h}\right)^2}\right)-r1\right)$ $r1=\left(\frac{3\pi he^{\frac{1}{4}}+2\pi h\cosh\left(\frac{\pi}{2}\right)+\pi^2 h\sinh\left(\frac{\pi}{2}\right)-2\pi h+26}{2\pi h}\right)$
	Present theory 2	$\frac{2z}{13}\cdot\left(\cosh\left(\frac{\pi z}{h}\right)++e^{\left(\frac{z}{h}\right)^2}+\frac{4z^2}{\pi(z^2h+h^3)}-r2\right)$ $r2=0.340334313$
	Present theory 3	$z-\frac{13}{16}z\cos\left(\frac{\pi}{8}\right)-\left(\frac{h}{\pi}\right)\sin\left(\frac{8\pi z^3}{h(4z^2-9h^2)}\right)$

Table 3. Non-dimensional natural frequency ($\bar{\beta}$) results of aluminium-1/zirconia $(Al)_1/ZrO_2$ MT-FGM square plates, in the case of homogeneous ceramic plate $\bar{\beta} = \omega h\sqrt{\rho_c/E_c}$.

	Ceramic		$p = 1$			$a/h = 5$		
Theories	$a/h = \sqrt{10}$	$a/h = 10$	$a/h = 5$	$a/h = 10$	$a/h = 20$	$p = 2$	$p = 3$	$p = 5$
3D Vel and Batra[77]	0.4658	0.0578	0.2192	0.0596	0.0153	0.2197	0.2211	0.2225
Quasi-3D HSDT Belabed et al.[14]	0.4659	0.0578	0.2192	0.0597	0.0153	0.2201	0.2214	0.2225
Present theory 2 (Quasi-3D)	0.4659	0.0578	0.2193	0.0597	0.0153	0.2201	0.2214	0.2225
Present theory 1 (Quasi-3D)	0.4660	0.0578	0.2193	0.0597	0.0153	0.2201	0.2214	0.2225
Quasi-3D Neves et al.[78]	–	–	0.2193	0.0596	0.0153	0.2198	0.2212	0.2225
Quasi-3D Neves et al.[79]	–	–	0.2193	0.0596	0.0153	0.2201	0.2216	0.2230

Table 4. Non-dimensional fundamental frequency ($\hat{\omega}$) results of aluminium-1/alumina $(Al)_1/Al_2O_3$ P-FGM square plates.

			Power-law index p				
a/h	Mode (m, n)	Theories	Ceramic	0.5	1	4	10
2	1(1,1)	Quasi-3D HSDT Belabed et al.[14]	0.9414	0.8248	0.7516	0.6056	0.5495
		Present theory 1 (Quasi-3D)	0.9411	0.8247	0.7514	0.6055	0.5494
		Present theory 2 (Quasi-3D)	0.9405	0.8242	0.7509	0.6063	0.5498
		Quasi-3D Matsunaga[13]	0.9400	0.8233	0.7477	0.5997	0.5460
		2D HSDT Thai and Kim[23]	0.9297	0.8110	0.7356	0.5924	0.5412
		Present theory 1 (2D)	0.9295	0.8109	0.7355	0.5926	0.5412
		Present theory 2 (2D)	0.9295	0.8108	0.7354	0.5938	0.5420
	2(1,2)	Quasi-3D HSDT Belabed et al.[14]	1.7512	1.5498	1.4164	1.1147	0.9958
		Present theory 1 (Quasi-3D)	1.7503	1.5491	1.4156	1.1143	0.9954
		Present theory 2 (Quasi-3D)	1.7558	1.5456	1.4123	1.1136	0.9937
		Quasi-3D Matsunaga[13]	1.7406	1.5425	1.4078	1.1040	0.9847
		2D HSDT Thai and Kim[23]	1.7233	1.5192	1.3844	1.0919	0.9807
		Present theory 1 (2D)	1.7219	1.5183	1.3834	1.0918	0.9802
		Present theory 2 (2D)	1.7198	1.5167	1.3818	1.0926	0.9800
5	1(1,1)	Present theory 2 (Quasi-3D)	0.2122	0.1826	0.1660	0.1409	0.1319
		Present theory 1 (Quasi-3D)	0.2122	0.1826	0.1660	0.1409	0.1318
		Quasi-3D HSDT Belabed et al.[14]	0.2121	0.1819	0.1640	0.1383	0.1306
		Quasi-3D Matsunaga[13]	0.2121	0.1819	0.1640	0.1383	0.1306
		2D HSDT Nguyen[29]	0.2117	0.1807	0.1634	0.1378	0.1303
		2D Belkhodja et al.[37]	0.2113	0.1808	0.1632	0.1378	0.1300
		Present theory 1 (2D)	0.2113	0.1807	0.1631	0.1378	0.1300
		2D HSDT Thai and Kim[23]	0.2113	0.1807	0.1631	0.1378	0.1301
		Present theory 2 (2D)	0.2113	0.1807	0.1631	0.1379	0.1301
	2(1,2)	Present theory 1 (Quasi-3D)	0.4663	0.4044	0.3679	0.3048	0.2812
		Quasi-3D HSDT Belabed et al.[14]	0.4659	0.4041	0.3676	0.3047	0.2811
		Present theory 2 (Quasi-3D)	0.4658	0.4041	0.3676	0.3046	0.2811
		Quasi-3D Matsunaga[13]	0.4658	0.4040	0.3644	0.3000	0.2790
		2D HSDT Nguyen[29]	0.4645	0.4004	0.3622	0.2981	0.2783
		2D Belkhodja et al.[37]	0.4625	0.3990	0.3609	0.2980	0.2769
		2D HSDT Thai and Kim[23]	0.4623	0.3989	0.3607	0.2980	0.2771
		Present theory 2 (2D)	0.4623	0.3989	0.3607	0.2980	0.2771
		Present theory 1 (2D)	0.4623	0.3989	0.3607	0.2979	0.2771
	3(2,2)	Present theory 1 (Quasi-3D)	0.6764	0.5896	0.5368	0.4382	0.4010
		Quasi-3D HSDT Belabed et al.[14]	0.6757	0.5890	0.5362	0.4381	0.4008
		Present theory 2 (Quasi-3D)	0.6754	0.5889	0.5360	0.4378	0.4005
		2D HSDT Thai and Kim[23]	0.6734	0.5836	0.5286	0.4291	0.3974
		2D Belkhodja et al.[37]	0.6694	0.5806	0.5258	0.4285	0.3946
		Present theory 1 (2D)	0.6689	0.5803	0.5255	0.4282	0.3948
		Present theory 2 (2D)	0.6688	0.5803	0.5254	0.4285	0.3948
		Quasi-3D Matsunaga[13]	0.6688	0.5803	0.5254	0.4284	0.3948
10	1(1,1)	Present theory 2 (Quasi-3D)	0.0578	0.0494	0.0449	0.0389	0.0369
		Present theory 1 (Quasi-3D)	0.0578	0.0494	0.0449	0.0389	0.0368
		Quasi-3D HSDT Belabed et al.[14]	0.0578	0.0494	0.0449	0.0389	0.0368
		Quasi-3D Matsunaga[13]	0.0578	0.0492	0.0443	0.0381	0.0364

(continued)

Table 4. (continued)

a/h	Mode (m, n)	Theories	Power-law index p				
			Ceramic	0.5	1	4	10
		Present theory 1 (2D)	0.0577	0.0490	0.0442	0.0381	0.0364
		Present theory 2 (2D)	0.0577	0.0490	0.0442	0.0381	0.0364
		2D HSDT Thai and Kim[23]	0.0577	0.0490	0.0442	0.0381	0.0364
		2D Belkhodja et al.[37]	0.0577	0.0490	0.0442	0.0381	0.0364
	2(1,2)	Present theory 1 (Quasi-3D)	0.1382	0.1185	0.1078	0.0923	0.0868
		Present theory 2 (Quasi-3D)	0.1382	0.1185	0.1077	0.0923	0.0869
		Quasi-3D HSDT Belabed et al.[14]	0.1381	0.1184	0.1077	0.0923	0.0868
		Quasi-3D Matsunaga[13]	0.1381	0.1180	0.1063	0.0905	0.0859
		Present theory 2 (2D)	0.1377	0.1175	0.1060	0.0903	0.0857
		2D HSDT Thai and Kim[23]	0.1377	0.1174	0.1059	0.0903	0.0856
		2D Belkhodja et al.[37]	0.1377	0.1174	0.1059	0.0902	0.0856
		Present theory 1 (2D)	0.1377	0.1174	0.1059	0.0902	0.0856
	3(2,2)	Present theory 1 (Quasi-3D)	0.2124	0.1827	0.1661	0.1410	0.1319
		Present theory 2 (Quasi-3D)	0.2124	0.1827	0.1661	0.1409	0.1320
		Quasi-3D HSDT Belabed et al.[14]	0.2121	0.1825	0.1659	0.1409	0.1318
		Quasi-3D Matsunaga[13]	0.2117	0.1810	0.1634	0.1378	0.1303
		Present theory 2 (2D)	0.2115	0.1809	0.1633	0.1379	0.1302
		2D HSDT Thai and Kim[23]	0.2113	0.1807	0.1631	0.1378	0.1301
		2D Belkhodja et al.[37]	0.2113	0.1807	0.1632	0.1378	0.1300
		Present theory 1 (2D)	0.2113	0.1807	0.1631	0.1378	0.1300
20	1(1,1)	Present theory 1 (Quasi-3D)	0.0148	0.0127	0.0115	0.0100	0.0095
		Present theory 2 (Quasi-3D)	0.0148	0.0126	0.0115	0.0100	0.0095
		Quasi-3D HSDT Belabed et al.[14]	0.0148	0.0126	0.0115	0.0100	0.0095
		Present theory 2 (2D)	0.0148	0.0126	0.0113	0.0098	0.0094
		2D HSDT Thai and Kim[23]	0.0148	0.0125	0.0113	0.0098	0.0094
		2D Belkhodja et al.[37]	0.0148	0.0125	0.0113	0.0098	0.0094
		Quasi-3D Matsunaga[13]	0.0148	0.0125	0.0113	0.0098	0.0094
		2D HSDT Nguyen[29]	0.0148	0.0125	0.0113	0.0098	0.0094
		Present theory 1 (2D)	0.0148	0.0125	0.0113	0.0098	0.0094
	2(1,2)	Present theory 2 (Quasi-3D)	0.0366	0.0313	0.0284	0.0247	0.0235
		Present theory 1 (Quasi-3D)	0.0366	0.0313	0.0284	0.0247	0.0234
		Present theory 2 (2D)	0.0366	0.0310	0.0280	0.0242	0.0232
		2D Belkhodja et al.[37]	0.0365	0.0310	0.0279	0.0241	0.0231
		2D HSDT Nguyen[29]	0.0365	0.0310	0.0279	0.0241	0.0231
		Present theory 1 (2D)	0.0365	0.0310	0.0279	0.0241	0.0231
	3(2,2)	Present theory 2 (Quasi-3D)	0.0579	0.0495	0.0450	0.0391	0.0370
		Present theory 1 (Quasi-3D)	0.0579	0.0495	0.0450	0.0390	0.0369
		Present theory 2 (2D)	0.0578	0.0491	0.0443	0.0382	0.0366
		2D Belkhodja et al.[37]	0.0577	0.0490	0.0442	0.0381	0.0364
		2D HSDT Nguyen[29]	0.0577	0.0490	0.0442	0.0381	0.0364
		Present theory 1 (2D)	0.0577	0.0490	0.0442	0.0381	0.0364

Table 5. Non-dimensional fundamental frequency ($\bar{\omega}$) results of aluminium-1/alumina $(Al)_1/Al_2O_3$ P-FGM rectangular plates ($b = 2a$).

a/h	Mode (m, n)	Theories	Power-law index p				
			Ceramic	0.5	1	5	10
5	1(1,1)	FSDT Hosseini et al.[80]	3.4409	2.9322	2.6473	2.2528	2.1677
		2D TSDT Hosseini et al.[84]	3.4412	2.9347	2.6475	2.2272	2.1407
		Present theory 1 (2D)	3.4413	2.9347	2.6476	2.2268	2.1406
		Present theory 2 (2D)	3.4413	2.9347	2.6476	2.2275	2.1408
		2D HSDT Thai and Thuc[21]	3.4416	2.9350	2.6478	2.2260	2.1403
		2D Belkhodja et al.[37]	3.4417	2.9350	2.6480	2.2269	2.1401
	2(1,2)	FSDT Hosseini et al.[80]	5.2802	4.5122	4.0773	3.4492	3.3094
		2D TSDT Hosseini et al.[84]	5.2813	4.5180	4.0781	3.3938	3.2514
		Present theory 1 (2D)	5.2814	4.5181	4.0782	3.3931	3.2511
		Present theory 2 (2D)	5.2815	4.5181	4.0782	3.3945	3.2515

(continued)

Table 5. (continued)

a/h	Mode (m, n)	Theories	Power-law index p: Ceramic	0.5	1	5	10
		2D HSDT Thai and Thuc[21]	5.2822	4.5187	4.0787	3.3914	3.2506
		2D Belkhodja et al.[37]	5.2824	4.5188	4.0792	3.3932	3.2501
	3(1,3)	FSDT Hosseini et al.[80]	8.0710	6.9231	6.2636	5.2579	5.0253
		2D TSDT Hosseini et al.[84]	8.0749	6.9366	6.2663	5.1425	4.9055
		Present theory 2 (2D)	8.0751	6.9368	6.2664	5.1439	4.9057
		Present theory 1 (2D)	8.0752	6.9369	6.2665	5.1411	4.9051
		2D HSDT Thai and Thuc [21]	8.0772	6.9384	6.2678	5.1378	4.9044
	4(2,1)	FSDT Hosseini et al.[80]	9.7416	8.6926	7.8711	6.5749	5.7518
		2D TSDT Hosseini et al.[84]	10.1164	8.7138	7.8762	6.4074	6.0954
		Present theory 2 (2D)	10.1167	8.7140	7.8764	6.4094	6.0957
		Present theory 1 (2D)	10.1169	8.7143	7.8766	6.4054	6.0949
		2D HSDT Thai and Thuc[21]	10.1201	8.7167	7.8787	6.4010	6.0942
10	1 (1,1)	FSDT Hosseini et al.[80]	3.6518	3.0983	2.7937	2.3998	2.3197
		2D TSDT Hosseini et al.[84]	3.6518	3.0990	2.7937	2.3916	2.3110
		Present theory 1 (2D)	3.6518	3.0991	2.7937	2.3913	2.3109
		2D Belkhodja et al.[37]	3.6518	3.0991	2.7938	2.3913	2.3108
		2D HSDT Thai and Thuc[21]	3.6519	3.0991	2.7937	2.3912	2.3108
		Present theory 2 (2D)	3.6525	3.0995	2.7941	2.3917	2.3115
		2D HSDT Nguyen[29]	3.6533	3.0996	2.7946	2.3911	2.3118
	2(1,2)	FSDT Hosseini et al.[80]	5.7693	4.8997	4.4192	3.7881	3.6580
		2D TSDT Hosseini et al.[84]	5.7694	4.9014	4.4192	3.7682	3.6368
		Present theory 1 (2D)	5.7696	4.9016	4.4193	3.7675	3.6365
		2D HSDT Thai and Thuc[21]	5.7697	4.9016	4.4194	3.7673	3.6365
		2D Belkhodja et al.[37]	5.7697	4.9016	4.4194	3.7674	3.6364
		Present theory 2 (2D)	5.7711	4.9026	4.4203	3.7684	3.6381
		2D HSDT Nguyen[29]	5.7731	4.9031	4.4216	3.7671	3.6388
	3(1,3)	FSDT Hosseini et al.[80]	9.1876	7.8145	7.0512	6.0247	5.8086
		2D TSDT Hosseini et al.[84]	9.1880	7.8189	7.0515	5.9765	5.7575
		Present theory 1 (2D)	9.1884	7.8192	7.0517	5.9747	5.7568
		2D HSDT Thai and Thuc[21]	9.1887	7.8194	7.0519	5.9742	5.7566
		Present theory 2 (2D)	9.1924	7.8219	7.0543	5.9770	5.7606
	4(2,1)	FSDT Hosseini et al.[80]	11.8310	10.0740	9.0928	7.7505	7.4639
		2D TSDT Hosseini et al.[84]	11.8315	10.0810	9.0933	7.6731	7.3821
		Present theory 1 (2D)	11.8321	10.0815	9.0937	7.6704	7.3811
		2D HSDT Thai and Thuc[21]	11.8326	10.0818	9.0940	7.6696	7.3808
		Present theory 2 (2D)	11.8386	10.0859	9.0980	7.6742	7.3872
20	1(1,1)	FSDT Hosseini et al.[80]	3.7123	3.1456	2.8352	2.4425	2.3642
		2D Belkhodja et al.[37]	3.7123	3.1458	2.8353	2.4402	2.3618
		2D TSDT Hosseini et al.[84]	3.7123	3.1458	2.8352	2.4403	2.3619
		2D HSDT Thai and Thuc[21]	3.7123	3.1458	2.8353	2.4401	2.3618
		Present theory 1 (2D)	3.7124	3.1458	2.8353	2.4401	2.3618
		2D HSDT Nguyen[29]	3.7127	3.1455	2.8355	2.4401	2.3622
		Present theory 2 (2D)	3.7140	3.1469	2.8363	2.4419	2.3641
	2(1,2)	FSDT Hosseini et al.[80]	5.9198	5.0175	4.5228	3.8939	3.7681
		2D Belkhodja et al.[37]	5.9199	5.0180	4.5228	3.8881	3.7621
		2D HSDT Thai and Thuc[21]	5.9199	5.0180	4.5228	3.8881	3.7621
		Present theory 1 (2D)	5.9199	5.0180	4.5228	3.8881	3.7621
		2D TSDT Hosseini et al.[84]	5.9199	5.0180	4.5228	3.8884	3.7622
		2D HSDT Nguyen[29]	5.9209	5.0176	4.5234	3.8880	3.7629
		Present theory 2 (2D)	5.9240	5.0208	4.5255	3.8924	3.7678
		1					
	3(1,3)	FSDT Hosseini et al.[80]	9.5668	8.1121	7.3132	6.2903	6.0843
		2D TSDT Hosseini et al.[84]	9.5669	8.1133	7.3132	6.2760	6.0690
		2D HSDT Thai and Thuc[21]	9.5671	8.1135	7.3133	6.2753	6.0688
		Present theory 1 (2D)	9.5671	8.1135	7.3134	6.2753	6.0688
		Present theory 2 (2D)	9.5777	8.1207	7.3202	6.2866	6.0836
		1					
	4(2,1)	FSDT Hosseini et al.[80]	12.4560	10.5660	9.5261	8.1875	7.9166
		2D TSDT Hosseini et al.[84]	12.4562	10.5677	9.5261	8.1636	7.8909
		2D HSDT Thai and Thuc[21]	12.4565	10.5680	9.5263	8.1624	7.8905
		Present theory 1 (2D)	12.4566	10.5680	9.5263	8.1623	7.8905
		Present theory 2 (2D)	12.4745	10.5802	9.5379	8.1813	7.9153

Table 6. Non-dimensional natural fundamental frequency parameter ($\bar{\omega}$) results of aluminium-2/alumina $(Al)_2/Al_2O_3$ P-FGM square symmetric and non-symmetric sandwich plates (type A: with homogeneous softcore).

			Symmetric				Non-symmetric
a/h	*p*	Theories	1-0-1	2-1-2	1-1-1	1-2-1	2-2-1
5	0	Quasi 3D Akavci et al.[73]	0.8538	0.8538	0.8538	0.8538	0.8538
		Quasi 3D Bessaim et al.[81]	0.8529	0.8529	0.8529	0.8529	0.8529
		3D Li et al.[82]	0.8529	0.8529	0.8529	0.8529	0.8529
		2D Akavci et al.[73]	0.8494	0.8494	0.8494	0.8494	0.8494
		Present theory 3 (2D)	0.8493	0.8493	0.8493	0.8493	0.8493
	0.5	Quasi 3D Bessaim et al.[81]	1.3877	1.3328	1.2899	1.2288	1.2563
		Quasi 3D Akavci et al.[73]	1.3868	1.3312	1.2885	1.2287	1.2560
		2D Akavci et al.[73]	1.3801	1.3250	1.2827	1.2235	1.2485
		Present theory 3 (2D)	1.3830	1.3286	1.2858	1.2248	1.2505
		3D Li et al.[82]	1.3789	1.3206	1.2805	1.2258	1.2453
	1	Quasi 3D Bessaim et al.[81]	1.5237	1.4613	1.4088	1.3330	1.3694
		Quasi 3D Akavci et al.[73]	1.5221	1.4578	1.4050	1.3307	1.3676
		Present theory 3 (2D)	1.5182	1.4567	1.4045	1.3287	1.3627
		2D Akavci et al.[73]	1.5143	1.4506	1.3983	1.3249	1.3587
		3D Li et al.[82]	1.5090	1.4333	1.3824	1.3213	1.3420
	5	Quasi 3D Akavci et al.[73]	1.6658	1.6218	1.5671	1.4735	1.5267
		Present theory 3 (2D)	1.6591	1.6200	1.5690	1.4766	1.5225
		3D Li et al.[82]	1.6587	1.5801	1.5028	1.4267	1.4601
		2D Akavci et al.[73]	1.6568	1.6129	1.5588	1.4665	1.5160
		Quasi 3D Bessaim et al.[81]	1.5237	1.6257	1.5737	1.4810	1.5301
	10	Quasi 3D Akavci et al.[73]	1.6761	1.6442	1.5944	1.5002	1.5544
		Quasi 3D Bessaim et al.[81]	1.6754	1.6471	1.6006	1.5084	1.5574
		3D Li et al.[82]	1.6728	1.6091	1.5267	1.4410	1.4831
		Present theory 3 (2D)	1.6684	1.6412	1.5957	1.5041	1.5497
		2D Akavci et al.[73]	1.6671	1.6350	1.5858	1.4928	1.5435
10	0	Quasi 3D Akavci et al.[73]	0.9296	0.9296	0.9296	0.9296	0.9296
		Quasi 3D Bessaim et al.[81]	0.9290	0.9290	0.9290	0.9290	0.9290
		3D Li et al.[82]	0.9290	0.9290	0.9290	0.9290	0.9290
		2D Akavci et al.[73]	0.9278	0.9278	0.9278	0.9278	0.9278
		Present theory 3 (2D)	0.9278	0.9278	0.9278	0.9278	0.9278
	0.5	Quasi 3D Bessaim et al.[81]	1.5771	1.5310	1.4885	1.4179	1.4404
		Quasi 3D Akavci et al.[73]	1.5771	1.5307	1.4883	1.4181	1.4409
		Present theory 3 (2D)	1.5753	1.5294	1.4870	1.4163	1.4364
		2D Akavci et al.[73]	1.5741	1.5279	1.4857	1.4157	1.4356
		3D Li et al.[82]	1.5735	1.5259	1.4846	1.4166	1.4342
	1	Quasi 3D Bessaim et al.[81]	1.7281	1.6863	1.6420	1.5630	1.5843
		Quasi 3D Akavci et al.[73]	1.7280	1.6853	1.6408	1.5624	1.5843
		Present theory 3 (2D)	1.7261	1.6845	1.6403	1.5613	1.5793
		2D Akavci et al.[73]	1.7246	1.6820	1.6377	1.5596	1.5776
		3D Li et al.[82]	1.7223	1.6744	1.6305	1.5579	1.5704
	5	Quasi 3D Akavci et al.[73]	1.8452	1.8436	1.8181	1.7486	1.7595
		Quasi 3D Bessaim et al.[81]	1.8447	1.8446	1.8203	1.7514	1.7597
		Present theory 3 (2D)	1.8423	1.8425	1.8185	1.7497	1.7541
		3D Li et al.[82]	1.8420	1.8261	1.7896	1.7267	1.7273
		2D Akavci et al.[73]	1.8414	1.8397	1.8144	1.7452	1.7515
	10	Quasi 3D Akavci et al.[73]	1.8420	1.8544	1.8378	1.7757	1.7816
		Quasi 3D Bessaim et al.[81]	1.8411	1.8549	1.8397	1.7788	1.7816
		3D Li et al.[82]	1.8402	1.8399	1.8081	1.7481	1.7478
		Present theory 3 (2D)	1.8388	1.8527	1.8379	1.7770	1.7762
		2D Akavci et al.[73]	1.8383	1.8504	1.8339	1.7722	1.7737

Table 7. Non-dimensional natural fundamental frequency parameter ($\bar{\omega}$) results of aluminium-2/alumina $(Al)_2/Al_2O_3$ P-FGM square symmetric and non-symmetric sandwich plates (Type A: with homogeneous hardcore).

			Symmetric				Non-symmetric	
a/h	*p*	Theories	1-0-1	2-1-2	1-1-1	1-2-1	2-2-1	2-1-1
5	0	Quasi 3D Akavci et al.[73]	1.6790	1.6790	1.6790	1.6790	1.6790	–
		Quasi 3D Bessaim et al.[81]	1.6772	1.6772	1.6772	1.6772	1.6772	–
		3D Li et al.[82]	1.6771	1.6771	1.6771	1.6771	1.6771	–
		2D Akavci et al.[73]	1.6702	1.6702	1.6702	1.6702	1.6702	–
		Present theory 3 (2D)	1.6701	1.6701	1.6701	1.6701	1.6701	–

(continued)

Table 7. (continued)

			Symmetric				Non-symmetric	
a/h	*p*	Theories	1-0-1	2-1-2	1-1-1	1-2-1	2-2-1	2-1-1
	5	Quasi 3D Akavci et al.[73]	0.9001	0.9416	1.0017	1.1202	1.0657	–
		Quasi 3D Bessaim et al.[81]	0.8985	0.9403	1.0005	1.1194	1.0642	–
		2D Akavci et al.[73]	0.8953	0.9365	0.9958	1.1133	1.0531	–
		Present theory 3 (2D)	0.8943	0.9357	0.9954	1.1133	1.0528	–
		3D Li et al.[82]	0.8909	0.9336	0.9980	1.1190	1.0561	–
								–
	10	Quasi 3D Akavci et al.[73]	0.8771	0.9045	0.9562	1.0743	1.0228	–
		Quasi 3D Bessaim et al.[81]	0.8754	0.9031	0.9549	1.0734	1.0209	–
		2D Akavci et al.[73]	0.8725	0.8998	0.9508	1.0677	1.0093	–
		Present theory 3 (2D)	0.8714	0.8989	0.9502	1.0676	1.0090	–
		3D Li et al.[82]	0.8683	0.8923	0.9498	1.0729	1.0095	–
10	0	3D Li et al.[82]	1.8268	1.8268	1.8268	1.8268	1.8268	1.8268
		2D SSDPT Touratier[55]	1.8245	1.8245	1.8245	1.8245	1.8245	1.8245
		2D HSDT El Meiche et al.[38]	1.8245	1.8245	1.8245	1.8245	1.8245	1.8245
		2D Akavci et al.[73]	1.8245	1.8245	1.8245	1.8245	1.8245	1.8245
		2D PSDPT Reddy[52]	1.8245	1.8245	1.8245	1.8245	1.8245	1.8245
		Present theory 3 (2D)	1.8245	1.8245	1.8245	1.8245	1.8245	1.8245
		FSDPT[83,85,75]	1.8244	1.8244	1.8244	1.8244	1.8244	1.8244
	0.5	3D Li et al.[82]	1.4461	1.4861	1.5213	1.5767	1.5493	1.5084
		2D SSDPT Touratier[55]	1.4444	1.4842	1.5193	1.5745	1.5520	1.5126
		2D PSDPT Reddy[52]	1.4442	1.4841	1.5192	1.5745	1.5520	1.5125
		Present theory 3 (2D)	1.4442	1.4841	1.5192	1.5745	1.5472	1.5064
		2D HSDT El Meiche et al.[38]	1.4442	1.4841	1.5192	1.5746	1.5471	1.5064
		FSDPT[83,85,75]	1.4417	1.4816	1.5170	1.5727	1.5500	1.5104
	1	3D Li et al.[82]	1.2447	1.3018	1.3552	1.4414	1.3976	1.3351
		2D SSDPT Touratier[55]	1.2434	1.3002	1.3534	1.4393	1.4079	1.3489
		2D PSDPT Reddy[52]	1.2432	1.3001	1.3533	1.4393	1.4079	1.3489
		Present theory 3 (2D)	1.2432	1.3001	1.3533	1.4394	1.3957	1.3334
		2D HSDT El Meiche et al.[38]	1.2431	1.3000	1.3533	1.4394	1.3956	1.3333
		FSDPT[83,85,75]	1.2403	1.2973	1.3507	1.4372	1.4056	1.3464
	5	2D Akavci et al.[73]	0.9462	0.9820	1.0448	1.1740	1.1090	–
		2D SSDPT Touratier[55]	0.9463	0.9821	1.0448	1.1740	1.1474	1.0745
		2D PSDPT Reddy[52]	0.9460	0.9818	1.0447	1.1740	1.1473	1.0743
		Present theory 3 (2D)	0.9459	0.9818	1.0446	1.1740	1.1090	1.0306
		2D HSDT El Meiche et al.[38]	0.9457	0.9817	1.0446	1.1740	1.1088	1.0303
		3D Li et al.[82]	0.9448	0.9810	1.0453	1.1757	1.1098	1.0294
		FSDPT[83,85,75]	0.9426	0.9787	1.0418	1.1716	1.1447	1.0716
	10	2D SSDPT Touratier[55]	0.9288	0.9433	0.9952	1.1346	1.0415	1.0456
		2D Akavci et al.[73]	0.9286	0.9432	0.9956	1.1232	1.0612	–
		2D PSDPT Reddy[52]	0.9284	0.9430	0.9955	1.1231	1.1053	1.0386
		Present theory 3 (2D)	0.9283	0.9429	0.9955	1.1231	1.0610	0.9921
		2D HSDT El Meiche et al.[38]	0.9281	0.9428	0.9954	1.1231	1.0608	0.9918
		3D Li et al.[82]	0.9273	0.9408	0.9952	1.1247	1.0610	0.9893
		FSDPT[83,85,75]	0.9251	0.9396	0.9926	1.1207	1.1026	1.0358

Table 8. Non-dimensional natural fundamental frequency parameter ($\bar{\omega}$) results of aluminium-2/alumina $(Al)_2/Al_2O_3$ P-FGM square symmetric and non-symmetric sandwich plates (type A: with homogeneous hardcore) as well as ($p = 2$, $a/h = 10$).

		Mode (*m*, *n*)									
	Theories	(1,1)	(1,2)	(2,2)	(1,3)	(2,3)	(1,4)	(3,3)	(2,4)	(3,4)	(4,4)
1-2-1	3D Akavci et al.[73]	1.3051	3.1700	4.9385	6.0705	7.7061	9.7841	10.2870	11.2747	13.6465	16.7650
	2D El meiche et al.[38]	1.3025	3.1573	4.9098	6.0287	7.6415	9.6847	10.1782	11.1464	13.4665	16.5069
	Present theory 3 (2D)	1.3025	3.1572	4.9096	6.0283	7.6410	9.6837	10.1772	11.1452	13.4647	16.5042
	2D Akavci et al.[73]	1.3024	3.1569	4.9090	6.0275	7.6397	9.6816	10.1749	11.1425	13.4607	16.4984
	2D Zenkour[75]	1.3024	3.1569	4.9085	6.0262	7.6360	9.6712	10.1619	11.1232	13.4176	16.3982
2-2-1	2D Zenkour[75]	1.2678	3.0738	4.7807	5.8702	7.4400	9.4255	9.9044	10.8426	13.0826	15.9940
	3D Akavci et al.[73]	1.2509	3.0406	4.7399	5.8287	7.4033	9.4058	9.8908	10.8436	13.1336	16.1481
	2D Akavci et al.[73]	1.2439	3.0180	4.6968	5.7698	7.3181	9.2817	9.7564	10.6881	12.9227	15.8550
	Present theory 3 (2D)	1.2439	2.9768	4.6963	5.6224	7.2759	8.9872	9.7548	10.5344	12.8791	15.8516
	2D El meiche et al.[38]	1.2438	3.0170	4.6946	5.7666	7.3132	9.2744	9.7485	10.6789	12.9101	15.8376
	FSDT Nguyen et al.[76]	1.2436	3.0163	4.6932	5.7648	7.3110	9.2719	9.7460	10.6764	12.9084	15.8383

$$\begin{Bmatrix} \varepsilon_x \\ \varepsilon_y \\ \varepsilon_z \\ \gamma_{yz} \\ \gamma_{xz} \\ \gamma_{xy} \end{Bmatrix} = \begin{Bmatrix} \dfrac{\partial u_0}{\partial x} \\ \dfrac{\partial v_0}{\partial y} \\ 0 \\ 0 \\ 0 \\ \dfrac{\partial u_0}{\partial y} + \dfrac{\partial v_0}{\partial x} \end{Bmatrix} - z \begin{Bmatrix} \dfrac{\partial^2 w_b}{\partial x^2} \\ \dfrac{\partial^2 w_b}{\partial y^2} \\ 0 \\ 0 \\ 0 \\ 2\dfrac{\partial^2 w_b}{\partial x \partial y} \end{Bmatrix} - \begin{Bmatrix} f(z)\dfrac{\partial^2 w_s}{\partial x^2} \\ f(z)\dfrac{\partial^2 w_s}{\partial y^2} \\ -g'(z)\varphi \\ -g(z)\left(\dfrac{\partial w_s}{\partial y} + \dfrac{\partial \varphi}{\partial y}\right) \\ -g(z)\left(\dfrac{\partial w_s}{\partial x} + \dfrac{\partial \varphi}{\partial x}\right) \\ 2f(z)\dfrac{\partial^2 w_s}{\partial x \partial y} \end{Bmatrix} \tag{7}$$

and

$$g'(z) = \frac{\mathrm{d}g(z)}{\mathrm{d}z} = \frac{\mathrm{d}^2 f(z)}{\mathrm{d}z^2}. \tag{8}$$

The stresses. The constitutive relations (stress–strain relations) described the linear mechanical behaviours of the FGM plates, and the linear stresses field are written in terms of the stiffness matrix as

$$\begin{Bmatrix} \sigma_x \\ \sigma_y \\ \sigma_z \\ \tau_{yz} \\ \tau_{xz} \\ \tau_{xy} \end{Bmatrix}^{(n)} = \begin{bmatrix} C_{11} & C_{12} & C_{13} & 0 & 0 & 0 \\ C_{12} & C_{22} & C_{23} & 0 & 0 & 0 \\ C_{13} & C_{23} & C_{33} & 0 & 0 & 0 \\ 0 & 0 & 0 & G_{44} & 0 & 0 \\ 0 & 0 & 0 & 0 & G_{55} & 0 \\ 0 & 0 & 0 & 0 & 0 & G_{66} \end{bmatrix}^{(n)} \begin{Bmatrix} \varepsilon_x \\ \varepsilon_y \\ \varepsilon_z \\ \gamma_{yz} \\ \gamma_{xz} \\ \gamma_{xy} \end{Bmatrix}^{(n)} \tag{9}$$

where the stiffness matrix includes stiffness coefficients, which are defined for 2D HSDT ($\epsilon_z = 0$) as

$$C_{11} = C_{22} = \frac{E(z)}{1-\nu^2} \tag{10a}$$

$$C_{12} = \nu . C_{11} \tag{10b}$$

$$C_{33} = C_{13} = C_{23} = 0 \tag{10c}$$

$$G_{44} = G_{55} = G_{66} = \frac{E(z)}{2(1+\nu)} \tag{10d}$$

Hence, for 3D and quasi-3D HSDT ($\epsilon_z \neq 0$) are given as

$$C_{11} = C_{22} = C_{33} = \frac{(1-\nu)E(z)}{(1-2\nu)(1+\nu)} \tag{11a}$$

$$C_{12} = C_{13} = C_{23} = \frac{\nu E(z)}{(1-2\nu)(1+\nu)} \tag{11b}$$

$$G_{44} = G_{55} = G_{66} = \frac{E(z)}{2(1+\nu)} \tag{11c}$$

The energy principle. The equations of motion are determined for deformable bodies by the Hamilton's principle that is formulated as

$$0 = \int_0^{t'} (\delta U - \delta K)\,\mathrm{d}t \tag{12}$$

where t' denotes a time period as well δU and δK are, respectively, the strain energy and kinetic energy variations of the FGM plates.

The strain energy. The strain energy (energy of internal loads) variation is calculated in equations (13) as follows, without the stretching effect ($\varphi = 0$):

$$\delta\ U = \int_V (\sigma_x \delta\ \varepsilon_x + \sigma_y \delta\ \varepsilon_y + \sigma_z \delta\ \varepsilon_z + \tau_{xy} \delta\ \gamma_{xy} + \tau_{yz} \delta\ \gamma_{yz} + \tau_{xz} \delta\ \gamma_{xz})\ \mathrm{d}V \tag{13a}$$

$$\begin{aligned}\delta\ U = \int_A \Bigg[& N_x \frac{\partial \delta u_0}{\partial x} - M_x^b \frac{\partial^2 \delta w_b}{\partial x^2} - M_x^s \frac{\partial^2 \delta w_s}{\partial x^2} + N_y \frac{\partial \delta v_0}{\partial y} - M_y^b \frac{\partial^2 \delta w_b}{\partial y^2} - M_y^s \frac{\partial^2 \delta w_s}{\partial y^2} + N_{xy} \left(\frac{\partial \delta u_0}{\partial y} + \frac{\partial \delta v_0}{\partial x} \right) \\ & -2M_{xy}^b \frac{\partial^2 \delta w_b}{\partial x \partial y} - 2M_{xy}^s \frac{\partial^2 \delta w_s}{\partial x \partial y} + S_{xz}^s \left(\frac{\partial \delta w_s}{\partial x} + \frac{\partial \delta \varphi}{\partial x} \right) + S_{yz}^s \left(\frac{\partial \delta w_s}{\partial y} + \frac{\partial \delta \varphi}{\partial y} \right) - N_z \delta \varphi \Bigg] \mathrm{d}A\end{aligned} \tag{13b}$$

where A, V and N, M, S denote, respectively, the section, the volume and the stresses resultants that are defined as in equations (14), without the stretching effect ($N_z = 0$):

$$\begin{bmatrix} N_x & N_y & 0 & 0 & 0 & N_{xy} \\ M_x^b & M_y^b & 0 & 0 & 0 & M_{xy}^b \\ M_x^s & M_y^s & 0 & 0 & 0 & M_{xy}^s \\ 0 & 0 & 0 & S_{yz}^s & S_{xz}^s & 0 \\ 0 & 0 & N_z & 0 & 0 & 0 \end{bmatrix} = \sum_{n=1}^{3} \int_{h_n}^{h_{n+1}} \begin{Bmatrix} 1 \\ z \\ f(z) \\ g(z) \\ g'(z) \end{Bmatrix} \{ \sigma_x \quad \sigma_y \quad \sigma_z \quad \tau_{yz} \quad \tau_{xz} \quad \tau_{xy} \}\,\mathrm{d}z \tag{14}$$

The kinetic energy. The kinetic energy variation is determined as in equations (15), without the stretching effect (φ=0):

$$\delta K = \int_{-h/2}^{h/2} \int_A (\dot{u}\delta\dot{u} + \dot{v}\delta\dot{v} + \dot{w}\delta\dot{w})\rho(z)\,\mathrm{d}A \tag{15a}$$

$$\begin{aligned}\delta K = \int_A \Bigg[& I_0 \Big(\dot{u}_0 \delta \dot{u}_0 + \dot{v}_0 \delta \dot{v}_0 + (\dot{w}_b + \dot{w}_s)(\delta \dot{w}_b + \delta \dot{w}_s) \Big) - I_1 \left(\dot{u}_0 \frac{\partial \delta \dot{w}_b}{\partial x} + \frac{\partial \dot{w}_b}{\partial x} \delta \dot{u}_0 + \dot{v}_0 \frac{\partial \delta \dot{w}_b}{\partial y} + \frac{\partial \dot{w}_b}{\partial y} \delta \dot{v}_{.0} \right) \\ & + I_2 \left(\frac{\partial \dot{w}_b}{\partial x} \frac{\partial \delta \dot{w}_b}{\partial x} + \frac{\partial \dot{w}_b}{\partial y} \frac{\partial \delta \dot{w}_b}{\partial y} \right) - J_1 \left(\dot{u}_0 \frac{\partial \delta \dot{w}_s}{\partial x} + \frac{\partial \dot{w}_s}{\partial x} \delta \dot{u}_0 + \dot{v}_0 \frac{\partial \delta \dot{w}_s}{\partial y} + \frac{\partial \dot{w}_s}{\partial y} \delta \dot{v}_{.0} \right) \\ & + J_2 \left(\frac{\partial \dot{w}_b}{\partial x} \frac{\partial \delta \dot{w}_s}{\partial x} + \frac{\partial \dot{w}_s}{\partial x} \frac{\partial \delta \dot{w}_b}{\partial x} + \frac{\partial \dot{w}_b}{\partial y} \frac{\partial \delta \dot{w}_s}{\partial y} + \frac{\partial \dot{w}_s}{\partial y} \frac{\partial \delta \dot{w}_b}{\partial y} \right) + K_2 \left(\frac{\partial \dot{w}_s}{\partial x} \frac{\partial \delta \dot{w}_s}{\partial x} + \frac{\partial \dot{w}_s}{\partial y} \frac{\partial \delta \dot{w}_s}{\partial y} \right) \\ & + J_1^s \Big((\dot{w}_b + \dot{w}_s) \delta \dot{\varphi} + \dot{\varphi} . \delta (\dot{w}_b + \dot{w}_s) \Big) + K_2^s \dot{\varphi} . \delta \dot{\varphi} \Bigg] \mathrm{d}A\,\mathrm{d}z\end{aligned} \tag{15b}$$

where the dot-superscript convention indicates the differentiation with respect to the time variable (t), the terms I_i, J_i and K_i denote the moments of inertia that are expressed as in equations (16), without the stretching effect $(J_1^s, K_2^s) = 0$:

$$(I_0, I_1, I_2, J_1, J_2, K_2, J_1^s, K_2^s) = \sum_{n=1}^{3} \int_{h_n}^{h_{n+1}} \rho(z)[1, z, z^2, f(z), zf(z), f^2(z), g(z), g^2(z)]\,\mathrm{d}z \tag{16}$$

The equations of motion:

The five equations of motion are found by substituting the energies variations (13 and 15) in the Hamilton's principle (12), then collecting the coefficients δu_0, δv_0, δw_0 and $\delta\varphi$ together, after integrating by parts every found term, they are appropriate to the five unknowns of the displacements field and the constitutive equations. The first equation of motion system is expressed in terms of displacements and strains as in equations (17), without the stretching effect ($N_z = 0$), ($\varphi = 0$), $(J_1^s, K_2^s) = 0$:

$$\delta u_0 : \quad \frac{\partial N_x}{\partial x} + \frac{\partial N_{xy}}{\partial y} = I_0 \ddot{u}_0 - I_1 \frac{\partial \ddot{w}_b}{\partial x} - J_1 \frac{\partial \ddot{w}_s}{\partial x} \tag{17a}$$

$$\delta v_0 : \quad \frac{\partial N_{xy}}{\partial x} + \frac{\partial N_y}{\partial y} = I_0 \ddot{v}_0 - I_1 \frac{\partial \ddot{w}_b}{\partial y} - J_1 \frac{\partial \ddot{w}_s}{\partial y} \tag{17b}$$

$$\delta w_b : \quad \frac{\partial^2 M_x^b}{\partial x^2} + 2\frac{\partial^2 M_{xy}^b}{\partial x \partial y} + \frac{\partial^2 M_y^b}{\partial y^2} = I_0(\ddot{w}_b + \ddot{w}_s) + I_1\left(\frac{\partial \ddot{u}_0}{\partial x} + \frac{\partial \ddot{v}_0}{\partial y}\right) - I_2 \nabla^2 \ddot{w}_b - J_2 \nabla^2 \ddot{w}_s + J_1^s \ddot{\varphi} \tag{17c}$$

$$\delta w_s : \quad \frac{\partial^2 M_x^s}{\partial x^2} + 2\frac{\partial^2 M_{xy}^s}{\partial x \partial y} + \frac{\partial^2 M_y^s}{\partial y^2} + \frac{\partial S_{xz}^s}{\partial x} + \frac{\partial S_{yz}^s}{\partial y} = I_0(\ddot{w}_b + \ddot{w}_s) + J_1\left(\frac{\partial \ddot{u}_0}{\partial x} + \frac{\partial \ddot{v}_0}{\partial y}\right) - J_2 \nabla^2 \ddot{w}_b - K_2 \nabla^2 \ddot{w}_s + J_1^s \ddot{\varphi} \tag{17d}$$

$$\delta \varphi : \quad \frac{\partial S_{xz}^s}{\partial x} + \frac{\partial S_{yz}^s}{\partial y} - N_z = J_1^s(\ddot{w}_b + \ddot{w}_s) + K_2^s \ddot{\varphi} \tag{17e}$$

where $\nabla^2 = (\partial^2/\partial x^2) + (\partial^2/\partial y^2)$ is the Laplacian operator in 2D Cartesian coordinates system.

When the stresses field (10) is substituted into the first stresses resultants (15), the second ones (18) are presented as a function of strain as in equations (18), without the stretching effect ($N_z = 0$), ($\varphi = 0$), (P, P^a, T, T^a)=0:

$$\begin{Bmatrix} N_x \\ N_y \\ N_{xy} \\ M_x^b \\ M_y^b \\ M_{xy}^b \\ M_x^s \\ M_y^s \\ M_{xy}^s \\ S_{yz}^s \\ S_{xz}^s \\ N_z \end{Bmatrix} = \begin{bmatrix} A_{11} & A_{12} & 0 & B_{11} & B_{12} & 0 & B_{11}^s & B_{12}^s & 0 & 0 & 0 & P \\ A_{12} & A_{22} & 0 & B_{12} & B_{22} & 0 & B_{12}^s & B_{22}^s & 0 & 0 & 0 & P \\ 0 & 0 & A_{66} & 0 & 0 & B_{66} & 0 & 0 & B_{66}^s & 0 & 0 & 0 \\ B_{11} & B_{12} & 0 & D_{11} & D_{12} & 0 & D_{11}^s & D_{12}^s & 0 & 0 & 0 & P^a \\ B_{12} & B_{22} & 0 & D_{12} & D_{22} & 0 & D_{12}^s & D_{22}^s & 0 & 0 & 0 & P^a \\ 0 & 0 & B_{66} & 0 & 0 & D_{66} & 0 & 0 & D_{66}^s & 0 & 0 & 0 \\ B_{11}^s & B_{12}^s & 0 & D_{11}^s & D_{12}^s & 0 & H_{11}^s & H_{12}^s & 0 & 0 & 0 & T \\ B_{12}^s & B_{22}^s & 0 & D_{12}^s & D_{22}^s & 0 & H_{12}^s & H_{22}^s & 0 & 0 & 0 & T \\ 0 & 0 & B_{66}^s & 0 & 0 & D_{66}^s & 0 & 0 & H_{66}^s & 0 & 0 & 0 \\ 0 & 0 & 0 & 0 & 0 & 0 & 0 & 0 & 0 & A_{44}^s & 0 & 0 \\ 0 & 0 & 0 & 0 & 0 & 0 & 0 & 0 & 0 & 0 & A_{55}^s & 0 \\ P & P & 0 & P^a & P^a & 0 & T & T & 0 & 0 & 0 & T^a \end{bmatrix} \begin{Bmatrix} \frac{\partial u_0}{\partial x} \\ \frac{\partial v_0}{\partial y} \\ \frac{\partial u_0}{\partial y} + \frac{\partial v_0}{\partial x} \\ -\frac{\partial^2 w_b}{\partial x^2} \\ -\frac{\partial^2 w_b}{\partial y^2} \\ -2\frac{\partial^2 w_b}{\partial x \partial y} \\ -\frac{\partial^2 w_s}{\partial x^2} \\ -\frac{\partial^2 w_s}{\partial y^2} \\ -2\frac{\partial^2 w_s}{\partial x \partial y} \\ \left(\frac{\partial w_s}{\partial y} + \frac{\partial \varphi}{\partial y}\right) \\ \left(\frac{\partial w_s}{\partial x} + \frac{\partial \varphi}{\partial x}\right) \\ \varphi \end{Bmatrix} \tag{18}$$

where the stiffness coefficients for quasi-3D HSDT ($\epsilon_z \neq 0$) areas in equations (19), without the stretching effect (P, P^a, T, T^a)=0:

$$\begin{Bmatrix} A_{11} & B_{11} & D_{11} & B^s_{11} & D^s_{11} & H^s_{11} & 0 & P & P^a & T & T^a \\ A_{12} & B_{12} & D_{12} & B^s_{12} & D^s_{12} & H^s_{12} & 0 & 0 & 0 & 0 & 0 \\ A_{66} & B_{66} & D_{66} & B^s_{66} & D^s_{66} & H^s_{66} & A^s_{44} & 0 & 0 & 0 & 0 \end{Bmatrix} = \sum_{n=1}^{3} \int_{h_n}^{h_{n+1}} [1, z, z^2, f(z), zf(z), [f(z)]^2, [g(z)]^2, g'(z), zg'(z), f(z)g'(z), [g'(z)]^2] \begin{Bmatrix} C_{11}(z) \\ C_{12}(z) \\ G(z) \end{Bmatrix} \mathrm{d}z, \tag{19a}$$

$$(A_{22}, B_{22}, D_{22}, B^s_{22}, D^s_{22}, H^s_{22}, A^s_{55}) = (A_{11}, B_{11}, D_{11}, B^s_{11}, D^s_{11}, H^s_{11}, A^s_{44}) \tag{19b}$$

By substituting the stresses resultants (18) into the first equations of motion system (17), the following simplified system is found as in equations (20), without the stretching effect ($N_z = 0$), ($\varphi = 0$), (P, P^a, T, T^a) $= 0$ $(J^s_1, K^s_2) = 0$:

$$\delta u_0: \quad A_{11}\frac{\partial^2 u_0}{\partial x^2} + A_{66}\frac{\partial^2 u_0}{\partial y^2} + (A_{12}+A_{66})\frac{\partial^2 v_0}{\partial x \partial y} - B_{11}\frac{\partial^3 w_b}{\partial x^3} - (B_{12}+2B_{66})\frac{\partial^3 w_b}{\partial x \partial y^2} - B^s_{11}\frac{\partial^3 w_s}{\partial x^3} - (B^s_{12}+2B^s_{66})\frac{\partial^3 w_s}{\partial x \partial y^2} + P\frac{\partial \varphi}{\partial x} = I_0 \ddot{u}_0 - I_1\frac{\partial \ddot{w}_b}{\partial x} - J_1\frac{\partial \ddot{w}_s}{\partial x} \tag{20a}$$

$$\delta v_0: \quad A_{22}\frac{\partial^2 v_0}{\partial y^2} + A_{66}\frac{\partial^2 v_0}{\partial x^2} + (A_{12}+A_{66})\frac{\partial^2 u_0}{\partial x \partial y} - B_{22}\frac{\partial^3 w_b}{\partial y^3} - (B_{12}+2B_{66})\frac{\partial^3 w_b}{\partial x^2 \partial y} - B^s_{22}\frac{\partial^3 w_s}{\partial y^3} - (B^s_{12}+2B^s_{66})\frac{\partial^3 w_s}{\partial x^2 \partial y} + P\frac{\partial \varphi}{\partial y} = I_0 \ddot{v}_0 - I_1\frac{\partial \ddot{w}_b}{\partial y} - J_1\frac{\partial \ddot{w}_s}{\partial y} \tag{20b}$$

$$\begin{aligned} \delta w_b: \quad & B_{11}\frac{\partial^3 u_0}{\partial x^3} + (B_{12}+2B_{66})\frac{\partial^3 u_0}{\partial x \partial y^2} + (B_{12}+2B_{66})\frac{\partial^3 v_0}{\partial x^2 \partial y} - B_{22}\frac{\partial^3 v_0}{\partial y^3} \\ & - D_{11}\frac{\partial^4 w_b}{\partial x^4} - D_{22}\frac{\partial^4 w_b}{\partial y^4} - 2(D_{12}+2D_{66})\frac{\partial^4 w_b}{\partial x^2 \partial y^2} - D^s_{11}\frac{\partial^4 w_s}{\partial x^4} - D^s_{22}\frac{\partial^4 w_s}{\partial y^4} \\ & - 2(D^s_{12}+2D^s_{66})\frac{\partial^4 w_s}{\partial x^2 \partial y^2} + P^a\left(\frac{\partial^2 \varphi}{\partial x^2} + \frac{\partial^2 \varphi}{\partial y^2}\right) = I_0(\ddot{w}_b + \ddot{w}_s) + I_1\left(\frac{\partial \ddot{u}_0}{\partial x} + \frac{\partial \ddot{v}_0}{\partial y}\right) \\ & - I_2\left(\frac{\partial^2 \ddot{w}_b}{\partial^2 x} + \frac{\partial^2 \ddot{w}_b}{\partial^2 y}\right) - J_2\left(\frac{\partial^2 \ddot{w}_s}{\partial^2 x} + \frac{\partial^2 \ddot{w}_s}{\partial^2 y}\right) + J^s_1 \ddot{\varphi} \end{aligned} \tag{20c}$$

$$\begin{aligned} \delta w_s: \quad & B^s_{11}\frac{\partial^3 u_0}{\partial x^3} + (B^s_{12}+2B^s_{66})\frac{\partial^3 u_0}{\partial x \partial y^2} + (B^s_{12}+2B^s_{66})\frac{\partial^3 v_0}{\partial x^2 \partial y} + B^s_{22}\frac{\partial^3 v_0}{\partial y^3} \\ & - D^s_{11}\frac{\partial^4 w_b}{\partial x^4} - D^s_{22}\frac{\partial^4 w_b}{\partial y^4} - 2(D^s_{12}+2D^s_{66})\frac{\partial^4 w_b}{\partial x^2 \partial y^2} + A^s_{44}\frac{\partial^2 w_s}{\partial y^2} + A^s_{55}\frac{\partial^2 w_s}{\partial x^2} \\ & - H^s_{11}\frac{\partial^4 w_s}{\partial x^4} - 2(H^s_{12}+2H^s_{66})\frac{\partial^4 w_s}{\partial x^2 \partial y^2} - H^s_{22}\frac{\partial^4 w_s}{\partial y^4} + T\left(\frac{\partial^2 \varphi}{\partial x^2} + \frac{\partial^2 \varphi}{\partial y^2}\right) + A^s_{44}\frac{\partial^2 \varphi}{\partial y^2} + \quad A^s_{55}\frac{\partial^2 \varphi}{\partial x^2} \\ = \; & I_0(\ddot{w}_b + \ddot{w}_s) + J_1\left(\frac{\partial \ddot{u}_0}{\partial x} + \frac{\partial \ddot{v}_0}{\partial y}\right) - J_2\left(\frac{\partial^2 \ddot{w}_b}{\partial^2 x} + \frac{\partial^2 \ddot{w}_b}{\partial^2 y}\right) - K_2\left(\frac{\partial^2 \ddot{w}_s}{\partial^2 x} + \frac{\partial^2 \ddot{w}_s}{\partial^2 y}\right) + J^s_1 \ddot{\varphi} \end{aligned} \tag{20d}$$

$$\delta\varphi: \quad P\left(\frac{\partial u_0}{\partial x}+\frac{\partial v_0}{\partial y}\right)-P^a\left(\frac{\partial^2 w_b}{\partial x^2}+\frac{\partial^2 w_b}{\partial y^2}\right)+(T-A_{44}^s)\frac{\partial^2 w_s}{\partial x^2}+(R-A_{55}^s)\frac{\partial^2 w_s}{\partial y^2}+T^a\varphi-A_{44}^s\frac{\partial^2\varphi}{\partial x^2}-A_{55}^s\frac{\partial^2\varphi}{\partial y^2}$$
$$= J_1^s(\ddot{w}_b+\ddot{w}_s)+K_2^s\ddot{\varphi} \tag{20e}$$

Navier approach for simply supported plates

In general, plates are classified in accordance with the used support type. Thus, in the present study, the following boundary conditions form for simply supported plate edges is imposed at the plate side edges as:

$$v_0(0,y)=w_b(0,y)=w_s(0,y)=\frac{\partial w_b}{\partial y}(0,y)=\frac{\partial w_s}{\partial y}(0,y)=0 \tag{21a}$$

$$v_0(a,y)=w_b(a,y)=w_s(a,y)=\frac{\partial w_b}{\partial y}(a,y)=\frac{\partial w_s}{\partial y}(a,y)=0 \tag{21b}$$

$$N_x(0,y)=M_x^b(0,y)=M_x^s(0,y)=N_x(a,y)=M_x^b(a,y)=M_x^s(a,y)=0 \tag{21c}$$

$$u_0(x,0)=w_b(x,0)=w_s(x,0)=\frac{\partial w_b}{\partial x}(x,0)=\frac{\partial w_s}{\partial x}(x,0)=0 \tag{21d}$$

$$u_0(x,b)=w_b(x,b)=w_s(x,b)=\frac{\partial w_b}{\partial x}(x,b)=\frac{\partial w_s}{\partial x}(x,b)=0 \tag{21e}$$

$$N_y(x,0)=M_y^b(x,0)=M_y^s(x,0)=N_y(x,b)=M_y^b(x,b)=M_y^s(x,b)=0 \tag{21f}$$

The Navier approach for simply supported boundary conditions is used to find analytical solutions of equations (20). The Navier approach solutions are partial differential equations in terms of displacements functions that satisfy the equations of boundary conditions (21), expressed by the following double-Fourier series for the plate with shear deformation model as in equations (22), without the stretching effect ($\varphi = 0$):

$$\begin{Bmatrix} u_0(x,y,t) \\ v_0(x,y,t) \\ w_b(x,y,t) \\ w_s(x,y,t) \\ \varphi(x,y,t) \end{Bmatrix} = \sum_{m=1}^{\infty}\sum_{n=1}^{\infty} e^{i\omega t} \begin{Bmatrix} U_{mn}\cos(\lambda x)\sin(\mu y) \\ V_{mn}\sin(\lambda x)\cos(\mu y) \\ W_{bmn}\sin(\lambda x)\sin(\mu y) \\ W_{smn}\sin(\lambda x)\sin(\mu y) \\ \Phi_{mn}\sin(\lambda x)\sin(\mu y) \end{Bmatrix} \tag{22}$$

where U_{mn}, V_{mn}, W_{bmn}, W_{smn} and Φ_{mn} are arbitrary determined parameters subjected to the conditions that the solution in (22) satisfies equations of motion (20), ω is the eigenfrequency associated with (m, n)th eigenmode of the plate for the free vibration analysis, $\lambda = mp/a$, $\mu = np/b$.

The double-Fourier series of displacements form (22) are substituted into the equations of motion system (20), and after some derivations and simplifications, the following equivalent system is obtained as in equations (23), without the stretching effect ($N_z = 0$), ($\varphi = 0$), (P, P^a, T, T^a)=0 $(J_1^s, K_2^s) = 0$:

$$([\mathrm{A}] - \omega^2\ [\mathrm{M}])\{\mathrm{R}\} = \{0\} \tag{23a}$$

$$\left(\begin{bmatrix} a_{11} & a_{12} & a_{13} & a_{14} & a_{15} \\ a_{12} & a_{22} & a_{23} & a_{24} & a_{25} \\ a_{13} & a_{23} & a_{33} & a_{34} & a_{35} \\ a_{14} & a_{24} & a_{34} & a_{44} & a_{45} \\ a_{15} & a_{25} & a_{35} & a_{45} & a_{55} \end{bmatrix} - \omega^2 \begin{bmatrix} m_{11} & 0 & m_{13} & 0 & 0 \\ 0 & m_{22} & m_{23} & m_{24} & 0 \\ m_{13} & m_{23} & m_{33} & m_{34} & m_{35} \\ 0 & m_{24} & m_{34} & m_{44} & m_{45} \\ 0 & 0 & m_{35} & m_{45} & m_{55} \end{bmatrix}\right) \begin{Bmatrix} U_{mn} \\ V_{mn} \\ W_{bmn} \\ W_{smn} \\ \Phi_{mn} \end{Bmatrix} = \begin{Bmatrix} 0 \\ 0 \\ 0 \\ 0 \\ 0 \end{Bmatrix} \tag{23b}$$

where the matrix [A] is

$$\begin{aligned}
a_{11} &= (\lambda^2 A_{11} + \mu^2 A_{66}),\\
a_{12} &= \lambda\mu(A_{12} + A_{66}),\\
a_{13} &= -\left(\lambda^3 B_{11} + \lambda\mu^2(B_{12} + 2B_{66})\right),\\
a_{14} &= -\left(\lambda^3 B^s_{11} + \lambda\mu^2(B^s_{12} + 2B^s_{66})\right),\\
a_{22} &= (\lambda^2 A_{66} + \mu^2 A_{22}),\\
a_{23} &= -\left(\mu^3 B_{22} + \lambda^2\mu(B_{12} + 2B_{66})\right),\\
a_{24} &= -\left(\mu^3 B^s_{22} + \lambda^2\mu(B^s_{12} + 2B^s_{66})\right),\\
a_{33} &= \left(\lambda^4 D_{11} + 2\lambda^2\mu^2(D_{12} + 2D_{66}) + \mu^4 D_{22}\right),\\
a_{34} &= \left(\lambda^4 D^s_{11} + 2\lambda^2\mu^2(D^s_{12} + 2D^s_{66}) + \mu^4 D^s_{22}\right),\\
a_{44} &= \left(\lambda^4 H^s_{11} + 2\lambda^2\mu^2(H^s_{12} + 2H^s_{66}) + \mu^4 H^s_{22} + \lambda^2 A^s_{55} + \mu^2 A^s_{44}\right),
\end{aligned} \tag{24a}$$

For the additional stretching effect

$$\begin{aligned}
a_{15} &= -P\lambda,\\
a_{25} &= -P\mu,\\
a_{55} &= (\lambda^2 A^s_{44} + \mu^2 A^s_{55} + T^a),
\end{aligned} \tag{24b}$$

As well the matrix [M] is

$$\begin{aligned}
m_{11} &= m_{22} = I_0,\\
m_{33} &= \left(I_0 + I_2(\lambda^2 + \mu^2)\right),\\
m_{34} &= \left(I_0 + J_2(\lambda^2 + \mu^2)\right),\\
m_{44} &= \left(I_0 + K_2(\lambda^2 + \mu^2)\right),
\end{aligned} \tag{24c}$$

For the additional stretching effect

$$\begin{aligned}
m_{13} &= -\lambda I_1,\\
m_{14} &= -\lambda J_1,\\
m_{23} &= -\mu I_1,\\
m_{24} &= -\mu J_1,\\
m_{35} &= m_{45} = J^s_1,\\
m_{55} &= K^s_2.
\end{aligned} \tag{24d}$$

Numerical examples, results and discussions

The present theory accuracy, novelty, simplicity and effectuality are evaluated for the free vibration analysis (the plate is not subjected to external loads) of both the square and rectangular, aluminium-1/alumina $(Al)_1/Al_2O_3$ and aluminium-1/zirconia $(Al)_1/ZrO_2$ P-FGM and MT-FGM monolayer plates in Tables 3 to 5 as well as square aluminium-2/alumina $(Al)_2/Al_2O_3$ P-FGM sandwich (symmetric as well as non-symmetric, with hardcore as well as softcore) plates in Tables 6 to 8 with simply supported edges. The obtained results were determined from the new developed hybrid HSDTs (polynomial–hyperbolic–exponential), (polynomial–trigonometric) and Belabed et al.,[14] El meiche et al.[38] theoretical formulation models. Many numerical examples investigated the different non-dimensional parameters effects such as the volume fraction index (p), the geometric ratios (a/h, a/b), the thickness ratio, the frequency modes (m, n) and the materials properties on the non-dimensional free vibration fundamental and natural frequencies ($\hat{\omega}$), ($\bar{\omega}$) and ($\bar{\beta}$). The results are compared with those generated by the FSDT,[74,76,80,83,85] the 3D and quasi-3D HSDT[13–14,73,77–79,81–82] and the 2D HSDT.[21,23,29,37,38,52,55,73,75,84]

For this study, the used matrices general form (23) analysed the free vibration problem as well the resulted non-dimensional mathematical relations are listed as:

For P-FGM and MT-FGM monolayer plates:

$$\bar{z} = \frac{z}{h},\ \bar{\beta} = \omega h\sqrt{\frac{\rho_m}{E_m}},\ \hat{\omega} = \omega h\sqrt{\frac{\rho_c}{E_c}},\ \bar{\omega} = \frac{\omega a^2}{h}\sqrt{\frac{\rho_c}{E_c}}, \tag{25a}$$

For P-FGM sandwich plates

$$\bar{z} = \frac{z}{h},\ \bar{\omega} = \frac{\omega a^2}{h}\sqrt{\frac{\rho_0}{E_0}}, \tag{25b}$$

where $\rho_0 = 1\ \text{kg/m}^3$ and $E_0 = 1$ GPa

Example 1. The natural frequency ($\bar{\beta}$) results are presented in Table 3, for homogeneous ceramic moderately stiff, softer, thick, moderately thick, thin and square $(Al)_1/ZrO_2$ MT-FGM plates, under the frequency modes ((m, n)=1(1,1), 2(1,2), 3(2,2)). It should be noted that the obtained results are in good agreement with all the mentioned theories solutions, especially with quasi-3D HSDT solutions of Belabed et al.[14] even for thick and softer MT-FGM plates, where ($\bar{\beta}$) becomes more important, and the produced maximum error between both the present theory 1, 2 solutions and Belabed et al.[14] is 0.0456% for ($a/h = 5$, $p = 1$), which is negligible.

Example 2. The fundamental frequency ($\hat{\omega}$) results are computed in Table 4, for homogeneous ceramic, stiffer, moderately stiff, softer, thick, moderately thick, thin, square $(Al)_1/Al_2O_3$ P-FGM plates, under the three frequency modes ((m, n) = 1(1,1), 2(1,2), 3(2,2)). The 2D HSDT 1 and 2 results are in very good agreement with all the presented theories solutions, especially with Belkhodja et al.[37] as well as Thai and Kim,[23] where the calculated maximum errors are, respectively, 0.0747% as well as 0.6683% and 0.7937%, these are an insignificant values obtained for ($p = 0$, $a/h = 5$,(m, n) = 3(2,2)) and ($a/h = 20$, $p = 0.5$,(m, n) = 1(1,1)). The 2D HSDT 1 results are identical to the others theories solutions, for thin and also moderately thin plates. The quasi-3-D HSDT 1 and 2 results are in well agreement with the others theories solutions, especially Belabed et al.,[14] where the maximum error

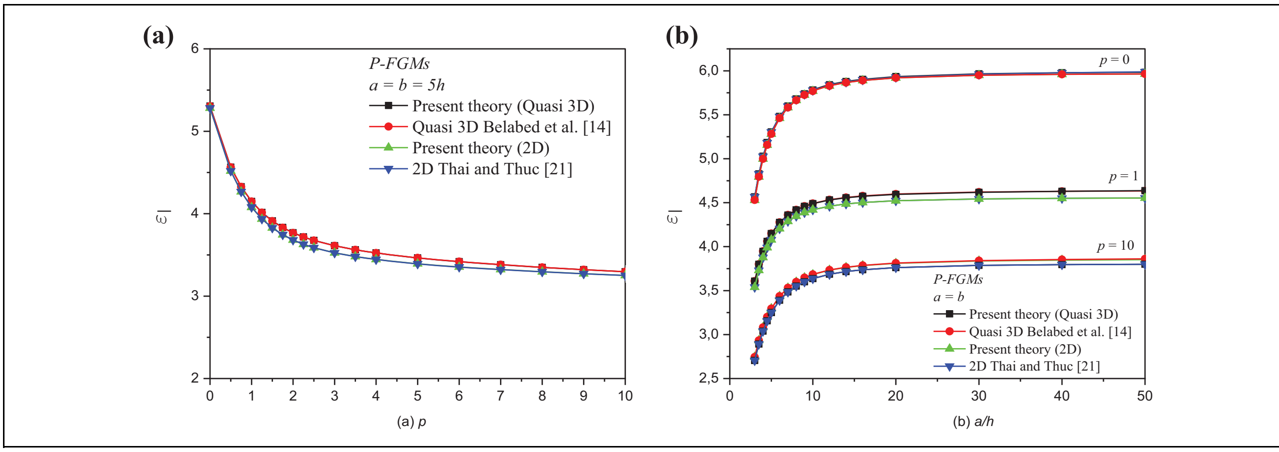

Figure 5. Non-dimensional fundamental frequency () variations for $(Al)_1/Al_2O_3$ P-FGM plates versus (a) the volume fraction index (*p*) and (b) the side-to-thickness ratio (*a*/*h*).

is 1.8453%, this is an insignificant value, obtained for ($p = 4$, $a/h = 5$, $(m, n) = (1,1)$). For thin plates, the quasi-3D HSDT results are very close to each other (the transverse shear deformation effect is not significant). Thus, the different theories solutions present more accuracy and convergence. It is to highlight that, the ($\hat{\omega}$) values increase with the index (p) and (a/h) ratio decrease, as well as the frequency modes increase.

Example 3. The fundamental frequency ($\bar{\omega}$) results are calculated in Table 5, for homogeneous ceramic, stiffer, moderately stiff, softer, thick, moderately thick, thin and rectangular $(Al)_1/Al_2O_3$ P-FGM plates under the frequency modes ($(m, n) = 1(1,1), 2(1,2), 3(1,3), 4(2,1)$). It can be observed that well agreement is presented between the both 2D HSDTs 1 and 2 solutions as well as the others theories, especially with Belkhodja et al.[37] where the maximum error computed is, respectively, 0.0308% and 0.1513% obtained for ($p = 10$, $a/h = 5$ and 20, mode 2), the maximum error in comparison with Hosseini et al.[84] is 0.0352% and 0.3083% obtained for ($p = 5$ and 10, $a/h = 10$ and 20, mode 4), as well the maximum error is, respectively, 0.0687% and 0.3133% in comparison with Thai and Thuc[21] obtained for ($p = 5$ and 10, $a/h = 5$ and 20, mode 4), these errors are insignificant. It is to highlight that, the ($\bar{\omega}$) values increase with the index (p) decreases as well as the increase of both the ratio (a/h) and the frequency modes that is clear in Figure 5.

Example 4. The fundamental frequency ($\bar{\omega}$) results are calculated in Table 7, for homogeneous ceramic, stiffer, moderately stiff, softer, thick, moderately thick and square $(Al)_2/Al_2O_3$ P-FGM symmetric and non-symmetric sandwich plates type A, with homogeneous hardcore.

It should be noted that the obtained results are in very good agreement with all the mentioned theories solutions, especially with Akavci et al.[73] and El Meiche et al.[38] solutions even for thin and stiffer P-FGM plates, where ($\bar{\omega}$) becomes more important, and the produced maximum error between both former theories and the present 2D theory 3 solutions is negligible, obtained as 0.1261% and 0.0302% for ($a/h = 5$, $p = 10$, (1-0-1)) and ($a/h = 10$, $p = 10$, (2-1-1)), respectively.

Example 5. The fundamental frequency ($\bar{\omega}$) results are again calculated in Table 8, for stiffer, moderately thick and square $(Al)_2/Al_2O_3$ P-FGM square symmetric and non-symmetric sandwich plates type A, with homogeneous hardcore, under 10 frequency modes ($(m, n) = 1(1,1), 2(1,2), 3(2,2), 4(1,3), 5(2,3), 6(1,4), 7(3,3), 8(2,4), 9(3,4), 10(4,4)$).

The 2D HSDT 3 results are in well agreement with all the presented theories solutions, especially with El Meiche et al.[38] and Akavci et al.[73] where the calculated maximum errors are, respectively, 3.0967% and 3.1729%. These are an insignificant values obtained for ($(m, n) = (1,4)$) and non-symmetric sandwich plates (2-2-1). The 2D HSDT 3 results are important for the frequency mode ($(m, n) = (4,4)$).

Example 6. The fundamental frequency ($\bar{\omega}$) results are presented also in Table 8, for stiffer, moderately stiff, thick, moderately thick and square $(Al)_2/Al_2O_3$ P-FGM square symmetric and non-symmetric sandwich plates type A, but with homogeneous softcore.

The 2D HSDT 3 results are in good agreement with all the presented theories solutions, especially with Akavci et al.[73] where the calculated maximum errors is 0.7513%, this is a negligible value obtained for ($a/h = 5$, $p = 10$, and non-symmetric sandwich plates (1-2-1)).

Conclusion

The developed three hybrid quasi-3D and 2D HSDTs analysed the free vibration problem of the isotropic, the MT-FGMs and P-FGMs, monolayer and sandwich (symmetric as well as non-symmetric, with hardcore as well as softcore) plates with simply supported edges, the theory investigated the displacements field of five unknowns, in which the transverse displacement membranes are the bending, the shear and the stretching through the plate thickness. The stretching displacement is in terms of the transverse shear deformation and stress that satisfied the stress-free boundary conditions on the plate free surfaces. The appropriate equations of motion are extracted from the Hamilton's principle and are solved by the Navier approach. The study of several parameters effects such as the volume fraction index, the geometric ratios, the frequency modes, and the materials properties on the natural frequencies are analysed. The proposed model reliability and accuracy, novelty, simplicity and effectuality of these new HSDTs are ascertained by comparisons of the calculated results with others plate theories solutions found in the literature references. As a conclusion, these theories are appropriate, simple, accurate and effective, as well as it gave the following results:

- It is obtained that the present formulations of polynomial–hyperbolic–exponential and polynomial–trigonometric forms can be further extended to all existing HSDTs models for numerous problems related to the shear deformable effect.
- The obtained results are in good agreement with the different others quasi-3D and 2D HSDT solutions in many cases that confirms the theory convergence.In the P-FGM plates, the ($\bar{\beta}$), ($\bar{\omega}$) and ($\hat{\omega}$) increase with the index (p) decreases.
- The increase in the fundamental frequencies ($\bar{\omega}$) and ($\hat{\omega}$) is influenced by the increase in the frequency modes.
- Furthermore, there is always a little difference between the quasi-3D results curve and the 2D results curves except for homogeneous ceramic plate ($p = 0$), where the quasi-3D results curve is underestimated in comparison with others ones and the reason is the stretching effect that is clear for softer and thick plates.

Acknowledgement

The authors thank Professor B Achour for their help and Editorial Office team and the reviewers for their valuable comments.

Declaration of conflicting interests

The author(s) declared no potential conflicts of interest with respect to the research, authorship, and/or publication of this article.

Funding

The author(s) received no financial support for the research, authorship, and/or publication of this article.

ORCID iD

Y Belkhodja https://orcid.org/0000-0002-9980-170X

References

1. Koizumi M. FGM activities in Japan. *Compos B Eng* 1997; 28B: 1–4.
2. Report from Science and Technology Agency of Japanese Government of 'Research on the basic technology for the development of functionally gradient materials for relaxation of thermal-stress' 1987.
3. Kawasaki A and Watanabe R. Powder metallurgical fabrication of the thermal-stress relief type of functionally gradient materials. '*Sintering '87 Tokyo'*, (Eds Somiya S., et al..), *Elsevier* 1988; 21: 197–1202.
4. Sasaki M, Wang Y, Hirano T, et al. Design of SiC/C functionally gradient material and its preparation by chemical vapor deposition. *J Ceram Soc Jpn* 1989; 97: 539–543.
5. Niino A and Maeda S. Recent development status of functionally gradient materials. *ISIJ Int* 1990; 30: 699–703.
6. Fukushima T, Kuroda S and Kitahara S. Gradient coatings formed by plasma twin torches and those properties. In: *Proceedings of the First International Symposium on Functionally Gradient Materials, Functionally Gradient Materials forum and the Society of Non-Traditional Technology*, Sendai, Tokyo, 1990, pp. 145–150.
7. Shimoda N, Kitaguchi S, Saito T, et al. Production of functionally gradient materials by applying low pressure plasma spray. In: *Proceedings of the First International Symposium on Functionally Gradient Materials, Functionally Gradient Materials Forum and the Society of Non-traditional Technology*, Sendai, Tokyo, 1990, pp. 151–156.
8. Sata N, Sanada N, Hirano T, et al. Fabrication of a functionally gradient material by using a self-propagating reaction process. In: *Proceedings of the First International Symposium on Combustion and Plasma Synthesis of High-Temperature Materials*, New Delhi, 1990, pp. 195–203. VCH Publishers, Inc.
9. Miyamoto Y, Nakanishi H, Tanaka I, et al. Gas pressure combustion sintering of TiC-Ni FGM. In: *Proceedings of the First International Symposium on Functionally Gradient Materials, Functionally Gradient Materials Forum and the Society of Non-traditional Technology*, Sendai, Tokyo, 1990, pp. 257–262.
10. Fukui Y. Fundamental investigation of functionally gradient material manufacturing system using centrifugal force. *Int J Japan Soc of Mech Eng Ser III* 1991; 34: 144–148.
11. Nishida IA. Thermoelectric energy conversion material. *FGM-News J FGM Forum* 1994; 24: 32–37.
12. Koizumi M and Niino M. Overview of FGM research in Japan. *MRS Bulletin* 1995; 20:19–21.
13. Matsunaga H. Free vibration and stability of functionally graded plates according to a 2-D higher-order deformation theory. *Compos Struct* 2008; 82: 499–512.
14. Belabed Z, Houari MSA, Tounsi A, et al. An efficient and simple higher order shear and normal deformation theory for functionally graded material (FGM) plates. *Compos B Eng* 2014; 274: 260–283.
15. Talha M and Singh BN. Static response and free vibration analysis of FGM plates using higher order shear deformation theory. *Appl Math Model* 2010; 34: 3991–4011.
16. Ait Atmane H, Tounsi A, Mechab I, et al. Free vibration analysis of functionally graded plates resting on Winkler-

Pasternak elastic foundations using a new shear deformation theory. *Int J Mech Mater Des* 2010; 6(2):113–121.
17. Qian LF, Batra RC and Chen LM. Static and dynamic deformations of thick functionally graded elastic plates by using higher-order shear and normal deformable plate theory and meshless local Petrov–Galerkin method. *Compos B Eng* 2004; 35: 685–697.
18. Younsi A, Tounsi A, Zaoui FZ, et al. Novel quasi-3D and 2D shear deformation theories for bending and free vibration analysis of FGM plates. *Geomech Eng Int J* 2018; 14(6): 519–532.
19. Hebali H, Tounsi A, Houari MSA, et al. New quasi-3D hyperbolic shear deformation theory for the static and free vibration analysis of functionally graded plates. *J Eng Mech* 2014; 140: 374–383.
20. Zaoui FZ, Tounsi A and Ouinas D. Free vibration of functionally graded plates resting on elastic foundations based on quasi-3D hybrid-type higher order shear deformation theory. *Smart Structures Systems* 2017; 20(4): 509–524.
21. Thai HT and Thuc P Vo. A new sinusoidal shear deformation theory for bending, buckling, and vibration of functionally graded plates. *Appl Math Model* 2013; 37: 3269–3281.
22. Neves AMA, Ferreira AJM, Carrera E, et al. Bending of FGM plates by a sinusoidal plate formulation and collocation with radial basis functions. *Mech Res Commun* 2011; 38: 368–731.
23. Thai HT and Kim SE. A simple higher-order shear deformation theory for bending and free vibration analysis of functionally graded plates. *Compos Struct* 2013; 96: 165–173.
24. Abedalnour M, Houari MSA, Tounsi A, et al. A novel quasi-3D trigonometric plate theory for free vibration analysis of advanced composite plates. *Compos Struct* 2018; 184: 688–697.
25. Neves AMA, Ferreira AJM, Carrera E, et al. A quasi-3D sinusoidal shear deformation theory for the static and free vibration analysis of functionally graded plates. *Compos B Eng* 2012; 43: 711–725.
26. Neves AMA, Ferreira AJM, Carrera E, et al. A quasi-3D hyperbolic shear deformation theory for the static and free vibration analysis of functionally graded plates. *Compos B Eng* 2012; 94: 1814–1825.
27. Thai CH, Ferreira AJM, Bordas SPA, et al. Isogeometric analysis of laminated composite and sandwich plates using a new inverse trigonometric shear deformation theory. *Europ J Mech/A Solid* 2014; 43(1): 89–108.
28. Thai CH, Kulasegaram S, Tran LV, et al. Generalized shear deformation theory for functionally graded isotropic and sandwich plates based on isogeometric approach. *Compos Struct* 2014; 141: 94–112.
29. Nguyen-Xuan H, Thai CH and Nguyen-Thoi T. Isogeometric finite element analysis of composite sandwich plates using a new higher order shear deformation theory. *Compos B Eng* 2013; 55(12): 558–574.
30. Thai CH, Ferreira AJM, Tran TD, et al. A size-dependent quasi-3D isogeometric model for functionally graded graphene platelet-reinforced composite microplates based on the modified couple stress theory. *Compos Struct* 2020: 234: 111695.
31. Thai CH, Zenkour A, Abdel-Wahab M, et al. A simple four-unknown shear and normal deformations theory for functionally graded isotropic and sandwich plates based on isogeometric analysis. *Compos Struct* 2016; 139: 77–95.
32. Thai CH, Ferreira AJM, Lee J, et al. An efficient size-dependent computational approach for functionally graded isotropic and sandwich microplates based on modifed couple stress theory and moving Kriging-based meshfree method. *Int J Mech Sci* 2018;142–143: 322–338.
33. Nebab M, Ait Atmane H, Bennai R, et al. Effect of nonlinear elastic foundations on dynamic behavior of FG plates using four-unknown plate theory. *Earthq Struct* 2019; 17 (5): 447–462.
34. Nguyen HX, Nguyen TN, Abdel-Wahab M, et al. A refined quasi-3D isogeometric analysis for functionally graded microplates based on the modified couple stress theory. *Comput Methods Appl Mech Engrg* 2016; 313: 904–940.
35. Bennoun M, Houari MSA and Tounsi A. A novel five variable refined plate theory for vibration analysis of functionally graded sandwich plate. *Mech Adv Mater Struct* 2016; 23(4): 423–431.
36. Zaoui F, Ouinas Z and Tounsi A. New 2D and quasi-3D shear deformation theories for free vibration of functionally graded plates on elastic foundations. *Compos B Eng* 2018; 159: 231–247.
37. Belkhodja Y, Ouinas D, Zaoui FZ, et al. An exponential-trigonometric higher order shear deformation theory (HSDT) for bending, free vibration, and buckling analysis of functionally graded materials (FGMs) plates. *Adv Compos Let* 2020; 29: 1–19.
38. El Meiche N, Tounsi A, Ziane N, et al. A new hyperbolic shear deformation theory for buckling and vibration of functionally graded sandwich plate. *Int J Mech Sci* 2011; 53(4): 237–247.
39. Jha DK, Tarun K and Singh RK. Higher order shear and normal deformation theory for natural frequency of functionally graded rectangular plates. *Nucl Eng Des* 2012; 250: 8–13.
40. Nguyen TK. A higher-order hyperbolic shear deformation plate model for analysis of functionally graded materials. *Int J Mech Mater Des* 2014; 11(2): 203–219.
41. Reddy JN. Analysis of functionally graded plates. *Int J Numer Meth Eng* 2000; 47(1-3): 663–684.
42. Benveniste Y. A new approach to the application of Mori–Tanaka's theory in composite materials. *Mech Mat* 1987; 6: 147–157.
43. Mori T and Tanaka K. Average stress in matrix and average elastic energy of materials with misfitting inclusions. *Acta Metall* 1973; 21: 571–574.
44. Kitipornchai S, Yang J and Liew KM. Random vibration of the functionally graded laminates in thermal environments. *Comp Meth Appl Mech Eng* 2006; 195: 1075–1095.
45. Tornabene F. Free vibration analysis of functionally graded conical, cylindrical shell and annular plate structures with a

four-parameter power-law distribution. *Comput Meth Appl Mech Eng* 2009; 198: 2911–2935.
46. Ambartsumian SA. On the theory of bending of anisotropic plates and shallow shells. *J Appl Mathe Mech* 1960; 24(2): 500–514.
47. Kaczkowski Z. *Plates - Statical calculations*. Warsaw: Arkady, 1968.
48. Panc V.*Theories of elastic plates. Mechanics of surface structure*, Vol. 2. Berlin: Springer Netherlands publisher, 1975, p. 740.
49. Reissner E. On transverse bending of plates, including the effect of transverse shear deformation. *Int J Solid Struct* 1975; 11(5): 569–573.
50. Levinson M. An accurate simple theory of the statics and dynamics of elastic plates. *Mech Res Commun* 1980; 7(6): 343–350.
51. Murthy MV. An improved transverse shear deformation theory for laminated anisotropic plates. NASA Technical Paper 1981; 1903.
52. Reddy JN. A simple higher order shear deformation theory for laminated composite plates. *J Appl Mech* 1984; 51(4): 745–753.
53. Levy M. Memoire sur la theorie des plaques elastique planes. *J de Mathematiques Pures et Appl* 1877; 30: 219–306.
54. Stein M. Nonlinear theory for plates and shells including the effect of transverse sharing. *AIAA J* 1986; 24(9): 1537–1544.
55. Touratier M. An efficient standard plate theory. *Int J Eng Sci* 1991; 29(8): 901–916.
56. Arya H, Shimpi R and Naik NK. A zigzag model for laminated composite beams. *Compos Struct* 2002; 56(1): 21–24.
57. Mantari JL, Oktem AS and Soares CG. A new trigonometric shear deformation theory for isotropic, laminated and sandwich plates. *Int J Solid Struct* 2012; (49): 43–53.
58. Grover N, Singh BN and Maiti DK. New nonpolynomial shear-deformation theories for structural behavior of laminated-composite and sandwich plates. *AIAA J* 2013; 51(8): 1861–1871.
59. Nguyen VH, Nguyen TK, Thai HT, et al. A new inverse trigonometric shear deformation theory for isotropic and functionally graded sandwich plates. *Compos B Eng* 2014; 66: 233–246.
60. Soldatos KP. A transverse shear deformation theory for homogeneous monoclinic plates. *Acta Mechanica* 1992; 94(3-4): 195–220.
61. Akavci SS and Tanrikulu AH. Buckling and free vibration analyses of laminated composite plates by using two new hyperbolic shear-deformation theories. *Mech Compos Mater* 2008; 44(2): 145–154.
62. Mahi A, AddaBedia EA, Tounsi A, et al. A new hyperbolic shear deformation theory for bending and free vibration analysis of isotropic, functionally graded, sandwich and laminated composite plates. *Appl Math Model* 2015; 39(9): 2489–2508.
63. Grover N, Maiti DK and Singh BN. A new inverse hyperbolic shear deformation theory for static and buckling analysis of laminated composite and sandwich plates. *Compos Struct* 2013; 95(1): 667–675.
64. Shi P, Dong C, Sun F, et al. A new higher order shear deformation theory for static, vibration and buckling responses of laminated plates with the isogeometric analysis. *Compos Struct* 2018. DOI:10.1016/j.compstruct.2018.07.080.
65. Karama M, Afaq KS and Mistou S. Mechanical behavior of laminated composite beam by the new multi-layered laminated composite structures model with transverse shear stress continuity. *Int J Solid Struct* 2003; 40(6): 1525–1546.
66. Aydogdu M. A new shear deformation theory for laminated composite plates. *Compos Struct* 2009; 89(1): 94–101.
67. Mantari JL, Oktem AS and Soares CG. Static and dynamic analysis of laminated composite and sandwich plates and shells by using a new higher-order shear deformation theory. *Compos Struct* 2011; 94(1): 37–49.
68. Mantari JL, Oktem AS and oares CG. A new higher order shear deformation theory for sandwich and composite laminated plates. *Compos B Eng* 2012; 43(3): 1489–1499.
69. Mantari JL and Guedes Soares C. Analysis of isotropic and multilayered plates and shells by using a generalized higher-order shear deformation theory. *Compos Struct* 2012; 94(8): 2640–2656.
70. Mantari JL, Granados E and Guedes Soares C. Vibrational analysis of advanced composite plates resting on elastic foundation. *Compos B Eng* 2014; 66: 407–419.
71. Suganyadevi S and Singh BN. Assessment of composite and sandwich laminates using a new shear deformation theory. *AIAA J* 2016; 54 (2): 784–787.
72. Singh DB and Singh BN. New higher order shear deformation theories for free vibration and buckling analysis of laminated and braided composite plates. *Int J Mech Sci* 2017; 67: 89–99.
73. Akavci SS. Mechanical behavior of functionally graded sandwich plates on elastic foundation. *Compos B Eng* 2016; 96: 136–152.
74. Reissner E. On the theory of bending of elastic plates. *J Math Phys* 1944; 23: 184–191.
75. Zenkour AM. A comprehensive analysis of functionally graded sandwich plates: Part 2D Buckling and free vibration. *Int J Solids Struct* 2005; 42(18-19): 5243–5258.
76. Nguyen TK, Vo TP and Thai HT. Vibration and buckling analysis of functionally graded sandwich plates with improved transverse shear stiffness based on the first-order shear deformation theory. *J Mech Enging Sci* 2014; 228(12): 2110–2131.
77. Vel SS and Batra RC. Three-dimensional exact solution for the vibration of functionally graded rectangular plates. *J Sound Vib* 2004; 272: 703–730.
78. Neves AMA, Ferreira AJM, Carrera E, et al. A quasi-3D sinusoidal shear deformation theory for the static and free vibration analysis of functionally graded plates. *Compos B Eng* 2012; 43: 711–725.
79. Neves AMA, Ferreira AJM, Carrera E, et al. A quasi-3D hyperbolic shear deformation theory for the static and free vibration analysis of functionally graded plates. *Compos B Eng* 2012; 94: 1814–1825.
80. Hosseini-Hashemi S, Fadaee M and Atashipour SR. A new exact analytical approach for free vibration of Reissner–

Mindlin functionally graded rectangular plates. *Int J Mech Sci* 2011; 53(1): 11–22.

81. Bessaim A, Houari MSA, Tounsi A, et al. A new higher order shear and normal deformation theory for the static and free vibration analysis of sandwich plates with functionally graded isotropic face sheets. *J Sand Struct Mat* 2013; 15(6): 671–703.
82. Li Q, Iu VP and Kou KP. Three-dimensional vibration analysis of functionally graded material sandwich plates. *J Sound Vib* 2008; 311: 498–515.
83. Reissner E. The effect of transverse shear deformation on the bending of elastic plates. *J Appl Mech* 1945; 12: 69–77.
84. Hosseini-Hashemi S, Fadaee M and Atashipour SR. Study on the free vibration of thick functionally graded rectangular plates according to a new exact closed-form procedure. *Compos Struct* 2011; 93: 722–735.
85. Mindlin RD. Influence of rotatory inertia and shear on flexural motions of isotropic elastic plates. *J Appl Mech* 1951; 18: 31–38.